Integrin-linked kinase is required for radial sorting of axons and Schwann cell remyelination in the peripheral nervous system

Jorge A. Pereira,[1] Yves Benninger,[1] Reto Baumann,[1] Ana Filipa Gonçalves,[1,2] Murat Özçelik,[1] Tina Thurnherr,[1] Nicolas Tricaud,[1] Dies Meijer,[3] Reinhard Fässler,[4] Ueli Suter,[1] and João B. Relvas[1,2]

[1]Institute of Cell Biology, Department of Biology, Eidgenössische Technische Hochschule Zurich, CH-8093 Zurich, Switzerland
[2]Instituto de Biologia Molecular e Celular, Universidade do Porto, 4150-180 Porto, Portugal
[3]Department of Cell Biology and Genetics, Erasmus MC University Medical Centre, 3000 DR Rotterdam, Netherlands
[4]Department of Molecular Medicine, Max Planck Institute of Biochemistry, D-82152 Martinsried, Germany

During development, Schwann cells (SCs) interpret different extracellular cues to regulate their migration, proliferation, and the remarkable morphological changes associated with the sorting, ensheathment, and myelination of axons. Although interactions between extracellular matrix proteins and integrins are critical to some of these processes, the downstream signaling pathways they control are still poorly understood. Integrin-linked kinase (ILK) is a focal adhesion protein that associates with multiple binding partners to link integrins to the actin cytoskeleton and is thought to participate in integrin and growth factor–mediated signaling. Using SC-specific gene ablation, we report essential functions for ILK in radial sorting of axon bundles and in remyelination in the peripheral nervous system. Our in vivo and in vitro experiments show that ILK negatively regulates Rho/Rho kinase signaling to promote SC process extension and to initiate radial sorting. ILK also facilitates axon remyelination, likely by promoting the activation of downstream molecules such as AKT/protein kinase B.

Introduction

Myelination of axons promotes neuronal survival and greatly increases the conduction velocity of nerve impulses. The control of Schwann cell (SC) differentiation and myelination derives at least in part from instructive cues originating within the extracellular environment. These signals include growth factors and proteins of the ECM as essential components (Colognato et al., 2005). Integrins, a major group of cell adhesion receptors for the proteins of the ECM, are composed of two noncovalently associated transmembrane glycoprotein subunits, α and β, both of which participate in the binding of ECM proteins. Ligand binding recruits cytoskeleton and signaling molecules to cell matrix contact sites where they link the actin cytoskeleton to the ECM and mediate signal transduction between the extracellular and the intracellular compartments (Hynes, 1992). In SCs, the genetic deletion of the β1-integrin gene (Feltri et al., 2002) causes defects in SC–axon contact and impairs the capacity of SCs to extend cytoplasmic processes into embryonic axon bundles to establish 1:1 relationships with individual axons, a process referred to as radial sorting. SC-specific deletion of FAK (Grove et al., 2007) or Rac1 (Benninger et al., 2007; Nodari et al., 2007), proteins involved in β1-integrin–mediated signaling, also results in deficient radial sorting. However, distinct cellular defects can underlie a common radial sorting phenotype. In FAK mutant nerves, impairment in radial sorting is likely to be caused by reduced SC proliferation and not by defects in SC–axon contact (Grove et al., 2007), similar to defects observed in SC-specific Cdc42 (cell division cycle 42)-deficient nerves (Benninger et al., 2007).

Integrin-linked kinase (ILK), a 52-kD protein identified and cloned based on its interaction with the β1-integrin cytoplasmic domain (Hannigan et al., 1996), is thought to be an essential regulator of integrin and growth factor–mediated

Correspondence to João B. Relvas: joao.relvas@cell.biol.ethz.ch

Abbreviations used in this paper: BL, basal lamina; CI, crush injury; *Dhh*, desert hedgehog; DRG, dorsal root ganglia; GSK3β, glycogen synthase kinase 3β; ILK, integrin-linked kinase; IPP, ILK–PINCH–parvin; MBP, myelin basic protein; MP, microtubule protection; PINCH, particularly interesting new Cys-His–rich protein; PLP, proteolipid protein; PNS, peripheral nervous system; ROCK, Rho kinase; SC, Schwann cell; SN, sciatic nerve.

Supplemental material can be found at:
http://doi.org/10.1083/jcb.200809008

The Rockefeller University Press $30.00
J. Cell Biol. Vol. 185 No. 1 147–161
www.jcb.org/cgi/doi/10.1083/jcb.200809008

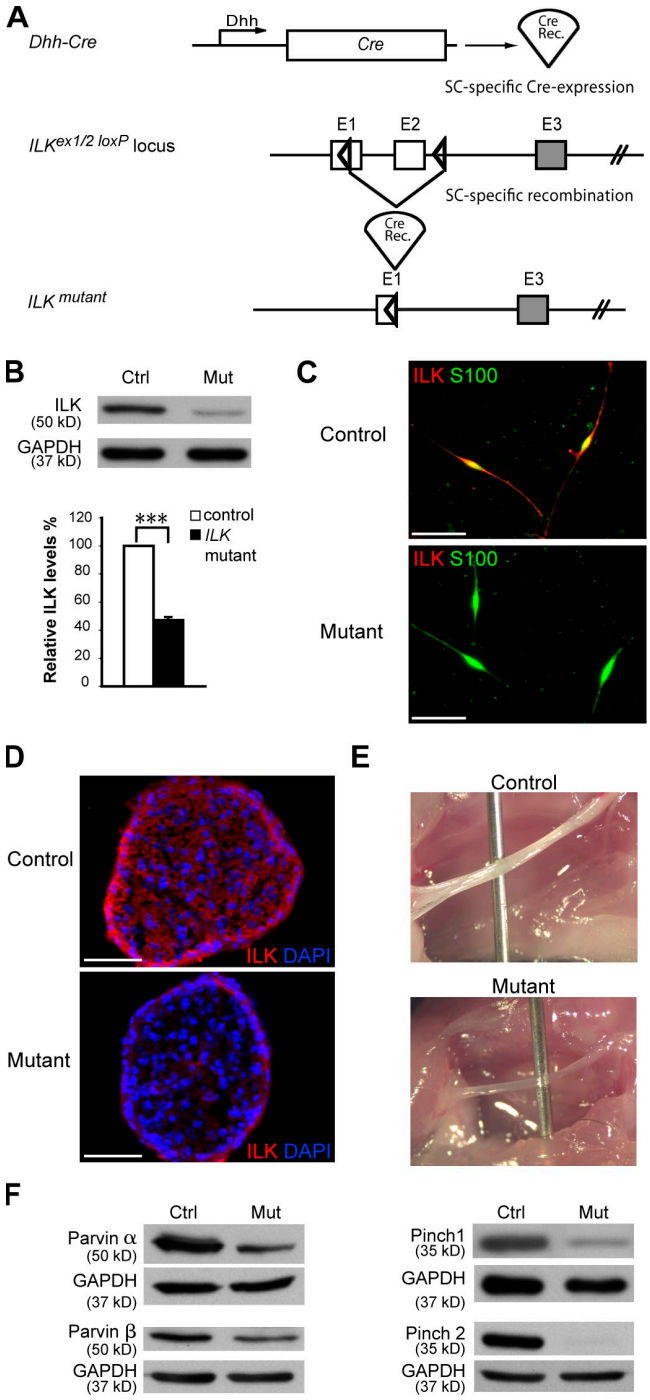

Figure 1. **Recombination of the conditional *ILK* allele in SCs of mutant mice.** (A) Regulatory sequences of the *Dhh* promoter drive the expression of the Cre recombinase (Cre Rec.) in SCs. Partial map of the *ILK* allele depicts the location of the loxP sequences. Upon Cre-mediated recombination, the genomic region located between the two loxP sites, which includes exon 2 and part of exon 1, is excised, thereby inactivating the conditional *ILK* allele. (B) Western blot analysis of protein lysates obtained from P1 SNs reveals a significant reduction in ILK levels compared with those of controls (Ctrl; $n = 3$, $P < 0.0001$). The low residual ILK protein levels detected in mutant (Mut) lysates are likely a result of the presence of endoneurial fibroblasts and some unrecombined SCs. Error bar indicates ± SEM. ***, $P < 0.001$. (C) Immunostaining of acutely plated SCs obtained from P1 control and mutant mice using antibodies for ILK and S100 (SC marker) reveals loss of ILK in mutant SCs. (D) Immunohistochemistry in E17.5 SN cryosections demonstrates loss of ILK in the mutant SCs in vivo. (E) Control and mutant SNs from P14 littermates. Note that mutant mice have thinner and more transparent SNs. (F) Upon conditional ablation of *ILK*, other protein members of the IPP complex (PINCH1 and 2 and parvin-α and -β) are reduced in P5 mutant SN lysates compared with controls. Bars, 50 µm.

signaling, functioning both as an adaptor protein and as a putative serine/threonine kinase. It consists of three domains: four N-terminal ankyrin repeats, a putative pleckstrin homology domain, and a C-terminal kinase domain. As an adaptor protein, ILK binds to particularly interesting new Cys-His–rich protein (PINCH) via its N-terminal domain and to parvins via its kinase domain to form a ternary complex that subsequently locates to cell–ECM adhesions. There, ILK binds the cytoplasmic domains of activated β1- and β3-integrin subunits, and the ILK–PINCH–parvin (IPP) complex can function as a signaling platform downstream of integrins by interfacing with the actin cytoskeleton and several different signaling pathways (Legate et al., 2006). The IPP complex can bind to filamentous actin via parvin and paxillin, which also binds directly to the ILK C-terminal kinase domain. Paxillin also binds to guanine nucleotide exchange factors, providing a connection between ILK and the GTPases of the Rho subfamily (Rosenberger et al., 2003) of which at least Cdc42 and Rac1 regulate SC development (Benninger et al., 2007; Nodari et al., 2007). Via PINCH, the complex can bind to the receptor tyrosine kinase–binding adaptor protein Nck-2 (Tu et al., 1998), establishing a potential direct link between ILK and growth factor signaling. Via its kinase domain, ILK is also thought to phosphorylate glycogen synthase kinase 3β (GSK3β) and AKT/PKB, which are involved in signaling pathways regulating proliferation, survival, and differentiation of different cell types (Legate et al., 2006), including SCs (Campana et al., 1999; Maurel and Salzer, 2000; Ogata et al., 2004). However, the direct phosphorylation of AKT/PKB by ILK is controversial (Legate et al., 2006).

In this study, we used conditional transgenic approaches in the mouse to investigate the roles of ILK in SC development in combination with cell culture experiments. We show that ILK is essential for radial sorting and axon remyelination and that the regulation of these two events is likely to require the activation of different signaling pathways.

Results

Conditional ablation of *ILK* in SCs

We conditionally ablated *ILK* by expressing Cre recombinase under the control of the desert hedgehog (*Dhh*) gene regulatory sequences (Fig. 1 A). Cre is active in SC precursors from embryonic day (E) 12 (Joseph et al., 2004). Recombination of the conditional *ILK* allele (Fig. 1 A) significantly reduced ILK in lysates obtained from sciatic nerves (SNs) of postnatal (P) day 1 mutant mice (Fig. 1 B). Loss of ILK also led to a strong reduction in the protein levels of the IPP complex members PINCH1, PINCH2, α-parvin, and β-parvin (Fig. 1 F). Cultured P1 mutant SCs were ILK negative in contrast to their control counterparts (Fig. 1 C). ILK immunoreactivity was strongly reduced in E17.5 mutant nerves compared with controls (Fig. 1 D). At P14, sciatic mutant

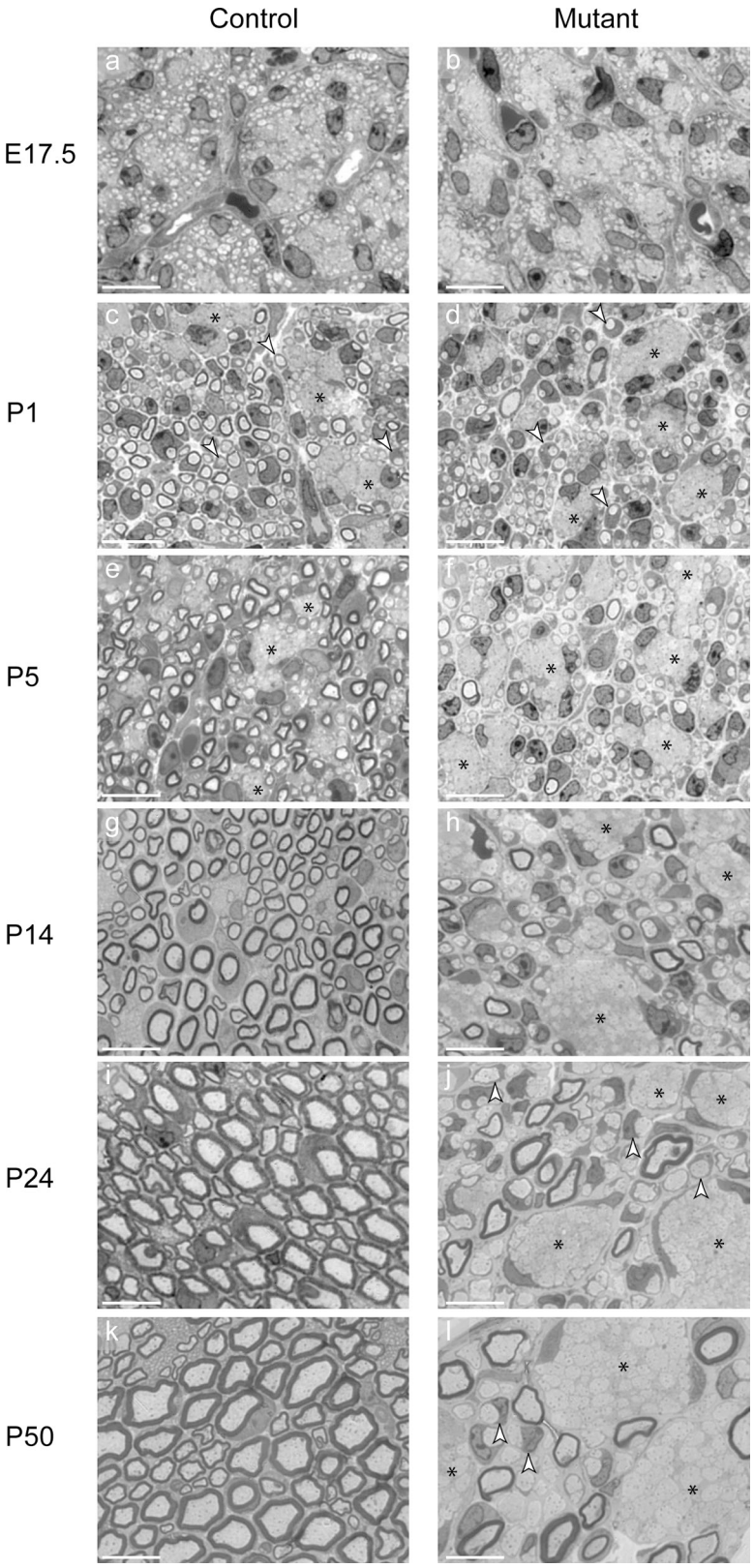

Figure 2. **Axonal sorting and myelination are impaired in *ILK* mutant SNs.** (a–l) 0.5-µm SN cross sections stained with Toluidine blue. Early in development (a–f), SCs are in close association with bundles of naked axons (c–f; asterisks). (c and d) Progressively individual axons are sorted from these bundles in a process referred to as radial sorting (arrowheads). (g, i, and k) In control nerves, individual large caliber axons are wrapped and myelinated. (h, j, and l) In the mutant nerves, radial sorting and myelination are impaired, and axon bundles persist into adulthood. Bars, 10 µm.

nerves were thinner and more transparent than controls (Fig. 1 E). ILK mutants displayed progressive hind limb paresis, which developed into paralysis at around P50. As a result of the severity of the phenotype and legal requirements, most experiments were performed at P24 or earlier.

Axon sorting and myelination deficits in *ILK* mutant nerves

During postnatal development, SCs progressively segregate and myelinate individual large caliber axons from axon bundles (Fig. 2, c, e, g, i, and k). At E17.5, SCs were present between bundles of

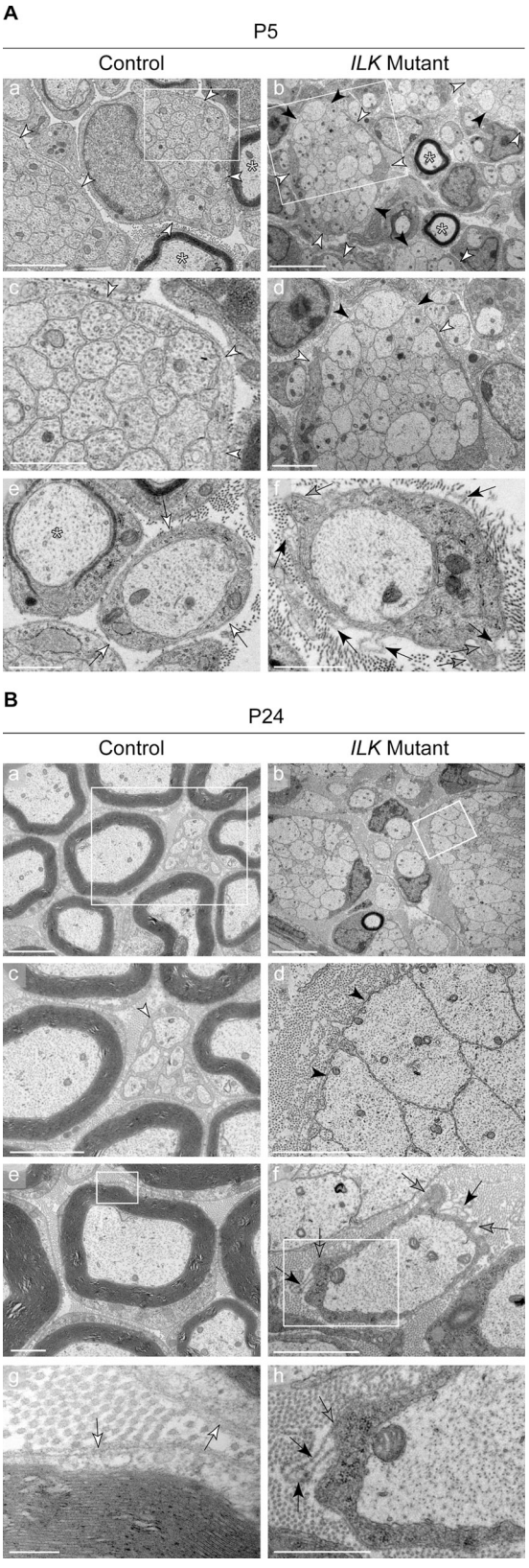

Figure 3. **Process extension and BL organization are impaired in *ILK* mutant SCs.** (A and B) EM micrographs of SN ultra-thin sections at P5 (A) and P24 (B). (A) At P5, immature SCs extend processes (white arrowheads) that fully envelop bundles of axons (a and c), which is a typical feature at this stage of maturation. In mutant nerves (b and d), SC processes often fail to completely enwrap axon bundles (black arrowheads). In controls, promyelinating SCs are surrounded by a tightly associated BL (e, white arrows). In contrast, mutant promyelinating SCs display cytoplasmic protrusions at the cell surface (f, gray arrows), frequently associated with a disorganized BL that forms loops detached from the plasma membrane (f, black arrows). Myelinating SCs could be found in controls, and some were also present in mutant nerves (asterisks). Bars: (b) 5 µm; (a and d) 2 µm; (c, e, f) 1 µm. (B) At P24, there are virtually no remaining axon bundles on the control nerves. Large caliber axons have been engaged and are myelinated (a, c, and e), whereas small caliber axons, which will not be myelinated during development, are engaged by nonmyelinating SCs (c, white arrowhead). In mutant nerves, axonal sorting is severely impaired, and many bundles persist. Mutant SCs associated with axon bundles fail to completely surround them (black arrowheads), resembling the phenotype observed at P5 (b and d). Unsorted axons are surrounded by loops of BL (black arrowheads). Control myelinating SCs reveal a tightly associated single BL (g, white arrows) in contrast to *ILK*-null cells in which multiple cytoplasmic protrusions (gray arrows) are visible (f), which are frequently associated with empty loops of BL (h; black arrows). Boxes indicate regions that are shown at a higher magnification in the panels below. Bars: (b) 5 µm; (a, c, d, and f) 2 µm; (e and h) 1 µm; (g) 0.2 µm.

tightly apposed axons in the SNs of control and mutant mice (Fig. 2, a and b). In P14 control mice (Fig. 2 g), large caliber axons were engaged in a 1:1 relationship with SCs. By P24, myelination was virtually complete (Fig. 2 i). In contrast, in the mutant nerves, axon sorting and myelination was impaired, and bundles of axons containing large caliber axons persisted at P50, the latest stage analyzed (Fig. 2 l). Few axons were myelinated in mutant nerves at all stages analyzed (Fig. 2, d, f, h, j, and l). Myelinating SCs in mutant nerves were not recombined, as they expressed both ILK and myelin basic protein (MBP; Fig. S2).

We conclude that the differentiation of mutant SCs is severely impaired. This conclusion is also supported by the findings that mutant nerves showed increased Oct6 immunoreactivity and reduced mRNA levels for several myelin genes compared with controls (Fig. S3, A and B).

ILK is required for proper extension and stabilization of SC processes

EM analysis at P5 showed that control and mutant nerves contained SCs at different stages of differentiation, including immature SCs associated with axon bundles, promyelinating SCs in a 1:1 relationship with large caliber axons, and SCs starting to myelinate. In control nerves, immature SCs extended long processes that fully enveloped axon bundles (Fig. 3 A, a and c). This was in contrast to mutant nerves in which immature SC processes often failed to completely envelop axon bundles (Fig. 3 A, b and d).

At the promyelinating stage, SC–axon profiles in control nerves were encircled by a tightly apposed basal lamina (BL; Fig. 3 A, e). In mutant nerves, these profiles contained aberrant cytoplasmic protrusions (Fig. 3 A, f). The surface of these protrusions was covered by BL. Often, empty loops of redundant BL, continuous with the apposed BL, were also present (Fig. 3 A, f). These loops are likely to be detached BL left behind by retracting protrusions, suggesting that SC processes repeatedly engaged and retracted from axons.

At P24, radial sorting in control nerves was completed (Fig. 3 B, a). Small caliber axons were engaged by nonmyelinating SCs (Fig. 3 B, c), and myelinating SCs were surrounded by an apposed BL (Fig. 3 B, e and g). Mutant nerves were severely hypomyelinated. Axon bundles in mutant nerves were still

not completely enveloped by immature SC processes (Fig. 3 B, b and d). As in P5 mutant nerves, layers of loose BL surrounded naked axon bundles and promyelinating SC–axon profiles (Fig. 3 B, d, f, and h).

We conclude that loss of ILK in SCs appears to lead to defects in process extension and stabilization. Such defects are likely to be the reason why radial sorting was impaired in mutant nerves.

ILK regulates SC process extension in a Rho kinase (ROCK)–dependent manner

As several studies link ILK to the regulation of Rho GTPase activity (Legate et al., 2006), we performed Rho GTPase activity assays in SN lysates (Benninger et al., 2007) obtained from P5 mutant and control mice. The expression levels of Cdc42 and Rac1 did not differ significantly between mutant and control nerves, but the activities of Cdc42 and Rac1 were significantly increased in mutant nerve lysates as compared with controls (Fig. 4 A). Rho activity was also significantly increased, but its expression levels were significantly decreased. ROCK (Riento and Ridley, 2003) is an effector of Rho, which inhibits neurite outgrowth in neurons (Luo, 2002) and outgrowth of processes in SCs (Melendez-Vasquez et al., 2004). Thus, we used ROCK inhibitors to investigate whether the shorter SC processes observed in mutant nerves were a consequence of increased ROCK activity.

Mutant SC cultures contained significantly more cells with shorter processes than those of control cultures (Fig. 4 B, a–c). Exposure to the selective ROCK inhibitors Y27632 (10 µM) or HA-1077 (fasudil; 40 µM; Melendez-Vasquez et al., 2004) increased the number of SCs with longer processes in both control and mutant cultures. However, control and mutant SCs no longer exhibited significant differences in SC process length (Fig. 4 B, d–i). The different concentrations used for fasudil and Y27632 might explain why SCs in cultures exposed to fasudil produced longer processes compared with those exposed to Y27632 (Fig. 4 B, f and i). We conclude that the shorter process length of mutant SCs is likely a result of increased Rho/ROCK activation. In addition, we used time-lapse video microscopy to evaluate the dynamics of control and mutant SC process extension and retraction. We recorded the behavior of SCs in control and mutant cultures in the presence or absence of fasudil over a period of 12 h (Videos 1–4 and Fig. S3 F). Our data show that the mean number of complete process retraction events per SC in mutant cultures is more than eight times higher than seen in controls or mutant cultures treated with fasudil (Fig. S3 F). There was no significant difference in the number of extension/retraction events among SCs of control, control treated with fasudil, or mutant treated with fasudil (Fig. S3 F). Overall, these results support the hypothesis that the loss of ILK regulates SC process extension and stabilization mainly via Rho/ROCK signaling.

In some cell types, ILK can negatively regulate Rho/ROCK activity by integrin-dependent FAK activation (Tahiliani et al., 1997; Wennerberg et al., 2000; Parsons, 2003) and paxillin phosphorylation (Chen et al., 2005). Accordingly, we show that in ILK mutant nerve lysates, the activation of FAK and paxillin were reduced as compared with controls (Fig. S4 A). In addition, using whole genome genechip arrays, we found that the mRNA levels of the atypical Rho GTPase RhoE, an important inhibitor of Rho/ROCK activity (Riento et al., 2003), were markedly reduced in *ILK* mutant nerves as compared with controls (unpublished data). Therefore, we analyzed the levels of RhoE in protein lysates obtained from *ILK* mutant and control nerves by Western blotting. Our results show that there was a dramatic reduction of RhoE expression levels in mutant lysates as compared with controls (Fig. S4 B, a). This reduction was confirmed by immunohistochemistry (Fig. S4 B, b) on cross sections obtained from control and mutant nerves and by immunocytochemistry in control and *ILK* mutant SCs in culture (Fig. S4 B, c).

Radial sorting is largely reestablished in the nerves of postnatal mutant ILK mice after injection of the ROCK inhibitor fasudil

To investigate whether inhibition of ROCK could reestablish radial sorting in mutant nerves, we injected mutant mice with either PBS or fasudil. Fasudil has been used to inhibit ROCK in vivo in various experimental settings (Mueller et al., 2005) and also in humans (Shimokawa et al., 2002). Injection of fasudil in control mice did not affect SC differentiation or myelination (Fig. 5 A, b). However, we found that fasudil treatment was able to reestablish radial sorting in the nerves of mutant mice (Fig. 5, A [d] and B [b and d]). Nerves of fasudil-injected mutant mice contained axon bundles of significantly smaller size than those of the PBS-injected mutant mice (Fig. 5 B, e). There was also a striking increase in the numbers of putative freshly sorted 1:1 SC–axon profiles in the nerves of fasudil-injected mutant mice (Fig. 5 B, b, d, and f). The numbers of myelinated fibers in PBS- or fasudil-injected mutant mice SNs, however, were not significantly different (Fig. 5 g). We conclude that inhibition of ROCK improves radial sorting but not myelination per se, suggesting that ILK function is also required for axonal myelination.

Reduced levels of phospho–Ser-473 of AKT/PKB in mutant nerves

Regulation of SC myelination, survival, and proliferation by SC–ECM interactions, exposure to neuregulin-1, PDGF, or IGF-1, or by axonal contact is thought to require AKT/PKB activation (Campana et al., 1999; Maurel and Salzer, 2000; Ogata et al., 2004; Nave and Salzer, 2006). AKT/PKB activation requires phosphorylation on Thr-308 and Ser-473. Although Thr-308 is phosphorylated by 3-phosphoinositide–dependent protein kinase-1, the identity of the Ser-473 kinase is unclear (Legate et al., 2006). One candidate is ILK, which has been shown to regulate phosphorylation of AKT/PKB on Ser-473 in different cell types (Persad et al., 2001; Troussard et al., 2003). Thus, we analyzed the levels of AKT/PKB phosphorylation of Ser-473 and Thr-308 in protein lysates obtained from ILK mutant and control nerves by Western blotting. Although at all stages analyzed the levels of AKT/PKB phosphorylation on Ser-473 in mutant lysates were significantly lower than those of their control counterparts, the levels of AKT/PKB phosphorylation on Thr-308 in mutant lysates were significantly higher than in controls (Fig. 6 A). Total levels of AKT/PKB were slightly reduced (Fig. 6 A).

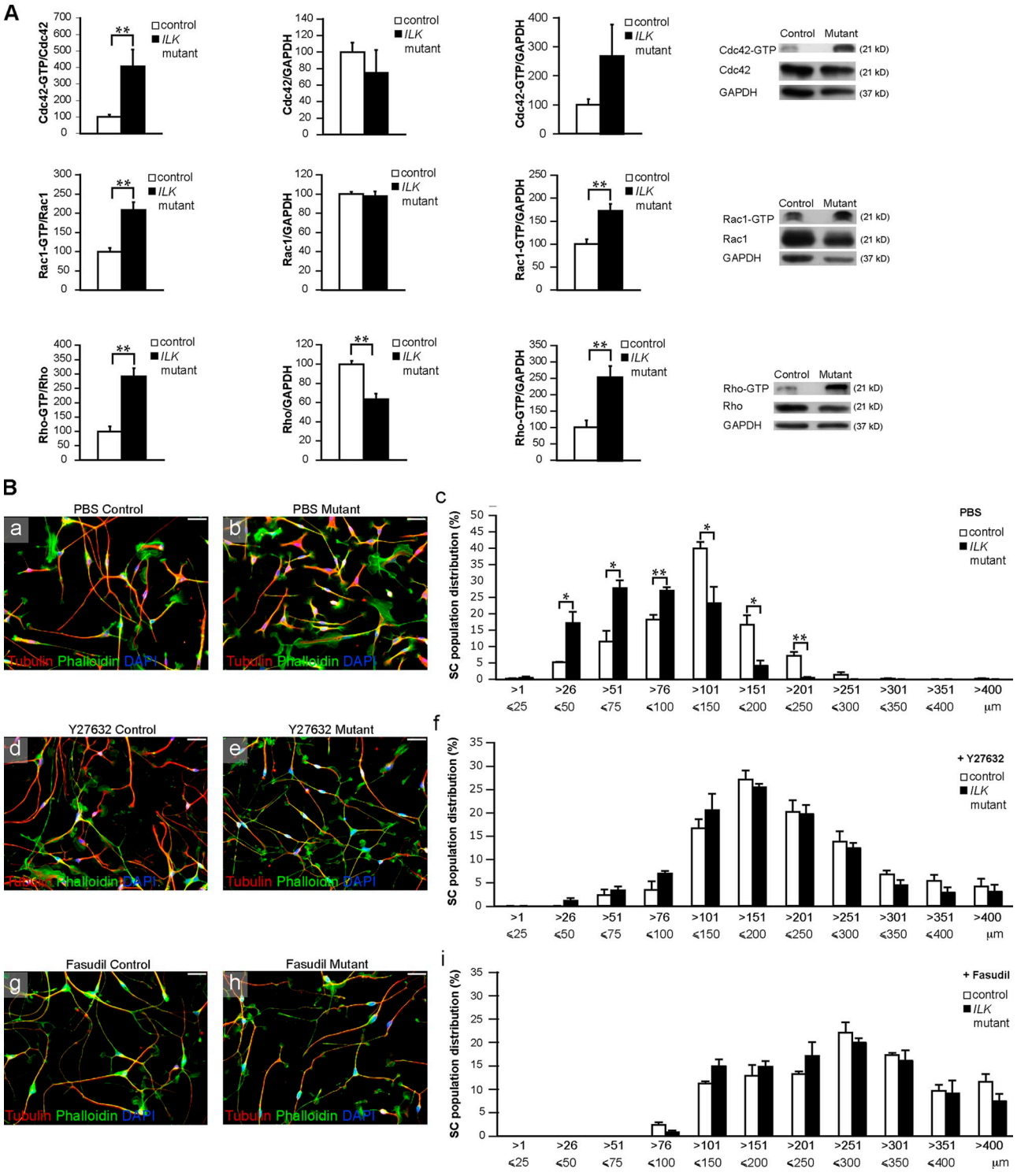

Figure 4. **ILK regulates SC process extension in a Rho/ROCK-dependent manner.** (A) Pull-down assays for active GTP-bound Rho GTPases using SN lysates obtained from P5 control and mutant mice. The activity of Cdc42 ($n = 4$, $P = 0.0096$) and Rac1 ($n = 4$, $P = 0.0012$) is significantly increased in mutant lysates, whereas their total expression levels are not. The amounts of activated Rac1 are more abundant in mutant than control SNs ($n = 4$, $P = 0.0017$), and although not statistically significant, the amounts of activated Cdc42 are also increased ($n = 4$, $P = 0.0511$). The aggregate activation of RhoA, B, and C ($n = 4$, $P = 0.0015$), termed Rho, is significantly increased in mutant lysates, whereas their total expression is significantly decreased ($n = 4$, $P = 0.0017$). Altogether, there is still more activated Rho protein in mutant than control SNs ($n = 4$, $P = 0.0050$). The Rho antibody used for Western blotting, after the coprecipitation with the recombinant rhotekin fragment, is not specific for individual Rho isoforms. (B, a and b, d and e, and g and h) Immunocytochemistry to reveal the cytoskeleton of control and mutant mouse SCs plated on laminin-2 for 24 h. Categorization of control and mutant SCs according to process length. (a–c) There is a higher frequency of SCs with shorter processes in mutant SC cultures as compared with control cultures ($n = 3$; $P_{26–50} = 0.026$; $P_{51–75} = 0.016$; $P_{76–100} = 0.0071$; $P_{101–150} = 0.036$; $P_{151–200} = 0.020$; $P_{201–250} = 0.0048$). Treatment of the SCs with the ROCK inhibitor Y27632 (d–f) or fasudil (g–i) restores process extension in mutant cells. Error bars indicate ± SEM. *, $P < 0.05$; **, $P < 0.01$. Bars, 20 μm.

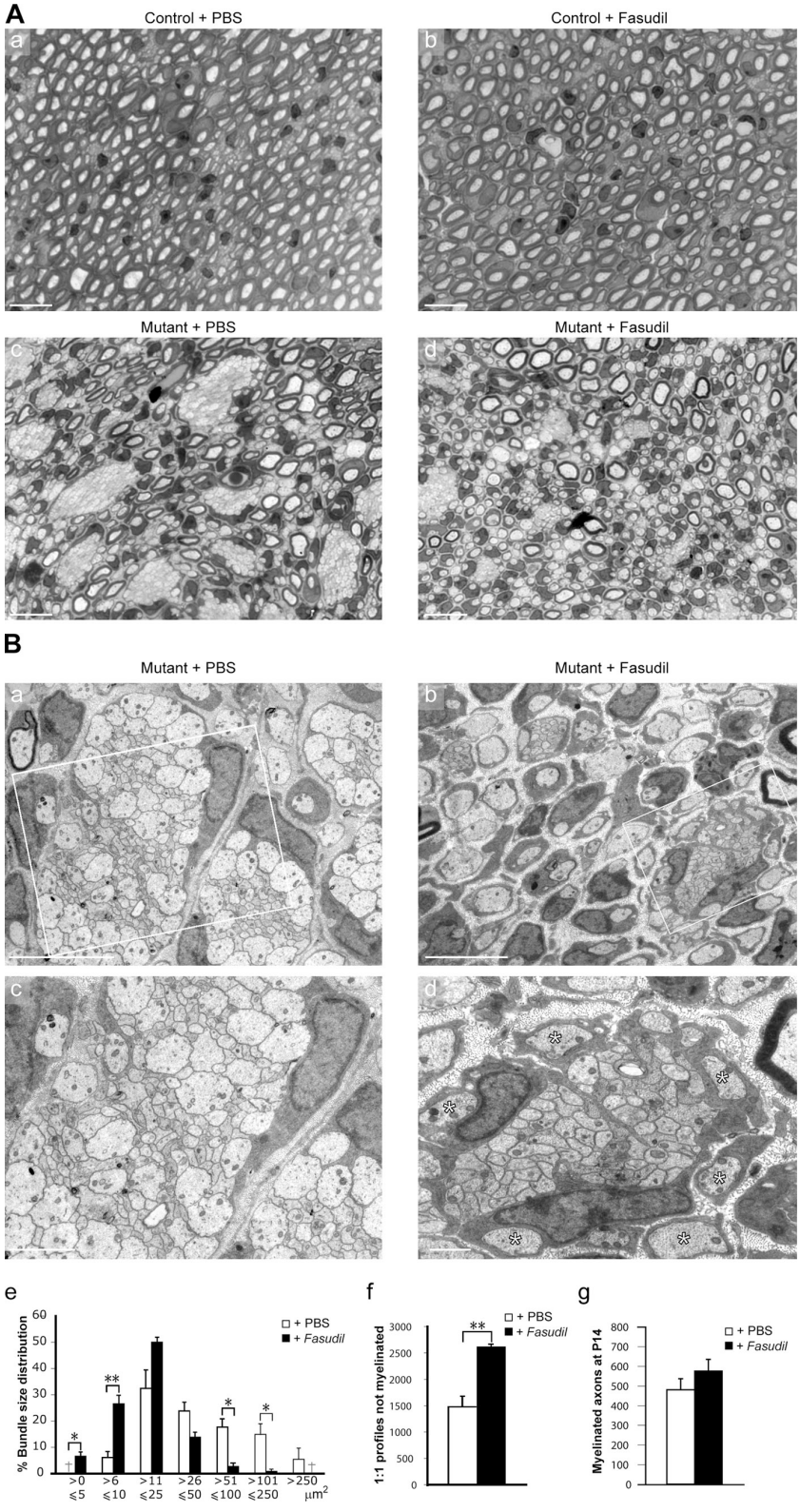

Figure 5. **Inhibition of ROCK signaling facilitates axonal sorting in *ILK* mutant mice.** *ILK* conditional control and mutant mice were injected i.p. with either PBS or 40 mg/kg/d fasudil over six consecutive days from P8 to P13. SNs were collected at P14. (A, a–d) Toluidine blue–stained 0.5-µm semithin sections of control and mutant animals injected with either fasudil or with PBS only. (a and b) There were no visible differences in myelination between fasudil- and PBS-injected control nerves. Bars, 10 µm. (B, a–d) Electron micrographs of mutant animals injected with either fasudil or with PBS only. PBS-injected mutant mice display large unsorted axonal bundles (a and c) as seen before, whereas bundles in fasudil-injected mutant mice are smaller (b and d; $n = 3$; $P_{0–5} = 0.012$; $P_{6–10} = 0.0064$; $P_{51–100} = 0.011$; $P_{101–250} = 0.027$). (e) Quantification of the unsorted bundle area reveals a higher frequency of small bundles in the fasudil-injected mice (6–25 µm^2) and a higher frequency of large bundles in PBS-injected mice (51 to >250 µm^2). Crosses indicate that no bundles within the size category were found in any of the animals analyzed. In the axonal bundle depicted in d, asterisks mark axons that have presumably been recently sorted and are larger than those remaining in the bundle. (f and g) There is a significant increase in the number of 1:1 relations in fasudil- versus PBS-injected mutant animals (f; $n = 3$, $P = 0.0052$); however, the total number of myelinated axons in the nerves analyzed does not differ between PBS- and fasudil-injected mice (g). Error bars indicate ± SEM. *, $P < 0.05$; **, $P < 0.01$. Boxes in a and b indicate regions that are shown at a higher magnification in c and d, respectively. Bars: (a and b) 5 µm; (c) 2 µm; (d) 1 µm.

Collectively, these results are consistent with the view that ILK regulates AKT/PKB activation during peripheral nervous system (PNS) myelination and that ILK function is required for phosphorylation of AKT/PKB on Ser-473 (Persad et al., 2001; Troussard et al., 2003).

Interestingly, the phosphorylation levels of GSK3β, another putative ILK substrate, remained unchanged in mutant nerves compared with controls (Fig. 6 B), suggesting that the mechanisms of AKT/PKB and GSK3β activation are different (Legate et al., 2006).

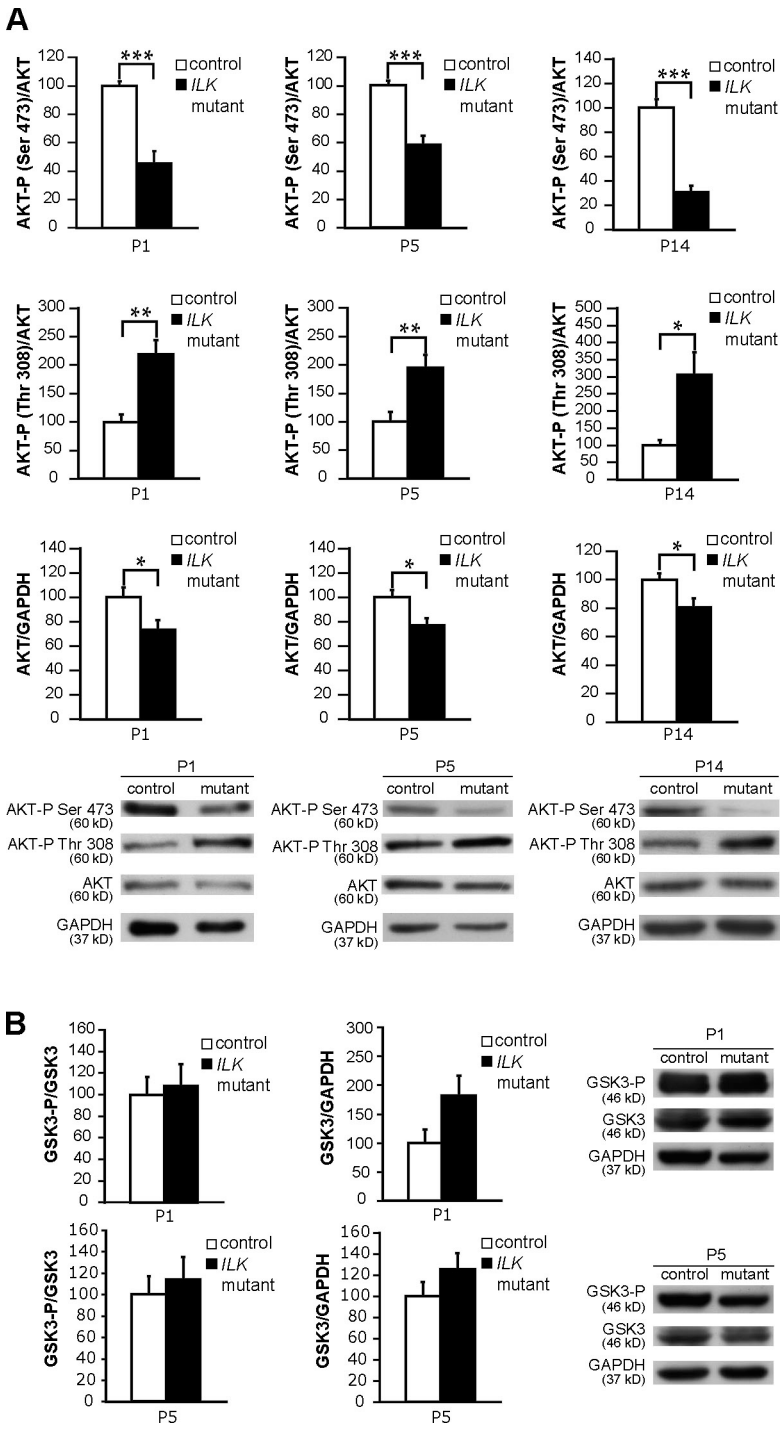

Figure 6. **ILK regulates PKB/AKT phosphorylation.** (A) AKT phosphorylation on Ser-473 is reduced in P1, P5, and P14 mutant nerves ($n = 4$, $P_{P1} = 0.00088$; $n = 4$, $P_{P5} = 0.00090$; $n = 5$, $P_{P14} < 0.0001$) unlike phosphorylation on Thr-308, which is higher in the mutants ($n = 6$; $P_{P1} = 0.0018$; $P_{P5} = 0.0062$; $P_{P14} = 0.010$). AKT total levels are slightly reduced in the mutants ($n = 10$, $P_{P1} = 0.027$; $n = 10$, $P_{P5} = 0.010$; $n = 11$, $P_{P14} = 0.019$). (B) GSK3β phosphorylation levels are not reduced in the absence of ILK either at P1 or P5. Error bars indicate ± SEM. *, $P < 0.05$; **, $P < 0.01$; ***, $P < 0.001$.

The formation of myelin sheaths after SN crush injury (CI) is impaired in *ILK* mutants

SN CI induces Wallerian degeneration in the nerve stump distal to the injury site followed by rapid axonal regeneration and remyelination (Chen et al., 2007). Radial sorting is no longer required before remyelination in contrast to developmental myelination. For these experiments, we used mutant and control mice expressing *CreERT2* (Indra et al., 1999; Li et al., 2000; Fig. 7 A) under the transcriptional control of the mouse proteolipid protein (PLP) gene regulatory elements (Leone et al., 2003). This transgene is transcriptionally active in SCs, and *CreERT2* translocates to the nucleus after injection of tamoxifen (Leone et al., 2003; Atanasoski et al., 2006). This allowed us to adjust the timing of *ILK* gene inactivation to our experimental requirements.

We injected 2-mo-old control and mutant mice with tamoxifen, and 2 mo later, crushed their SNs unilaterally. 7 d later, both noncrushed and crushed nerves were removed and lysed. Western blot analysis of these lysates confirmed that the levels of ILK in noncrushed and crushed mutant nerves were reduced compared with controls (Fig. 7 B). The loss of ILK in noninjured and injured nerves also led to a sizable reduction in

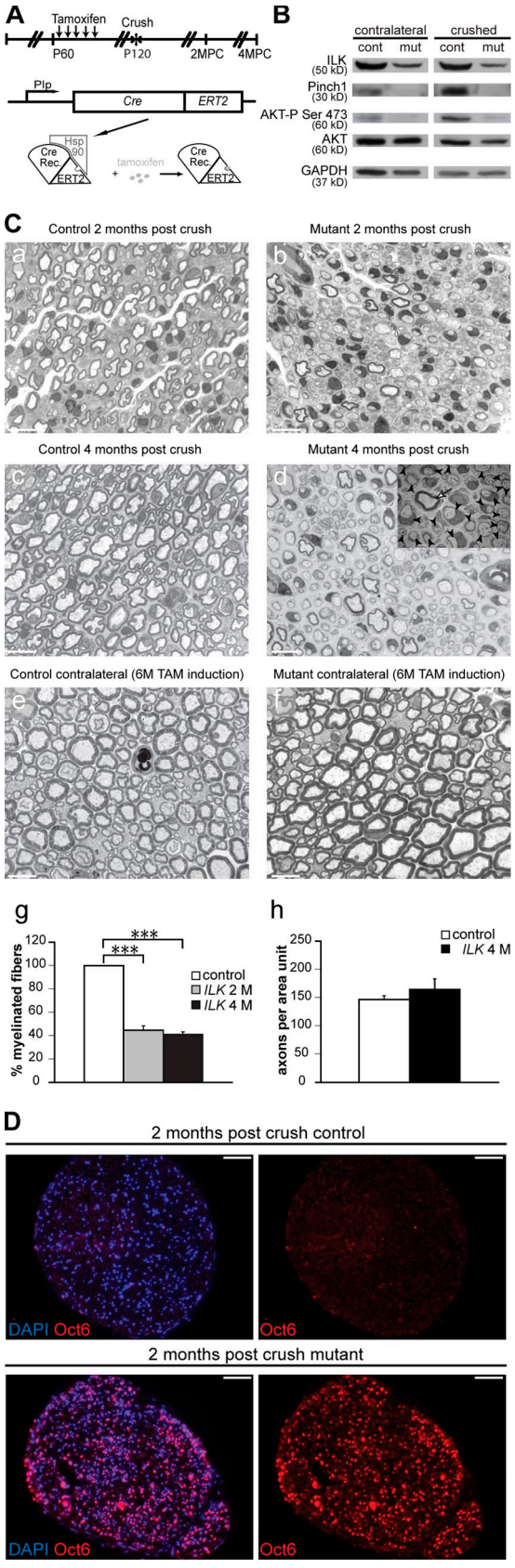

Figure 7. **ILK regulates PNS remyelination.** (A) Cre-mediated recombination was induced in 2-mo-old control and mutant mice by five daily consecutive tamoxifen injections. A period of 2 mo was allowed for recombination and protein depletion before assays were performed. Cre Rec., Cre recombinase; 2MPC, 2 mo post-CI; 4MPC, 4 mo post-CI. (B) Western blots performed on protein lysates obtained from contralateral and crushed nerves show a reduction in ILK levels in mutant (mut) nerves compared with those of controls (cont). PINCH1 and AKT phosphorylation levels are reduced in mutant nerves compared with controls. (C) Semithin sections of SNs collected 2 and 4 mo after CI. In contrast to controls (a, c, and g), mutant nerves show a significant reduction in the number of remyelinated axons at 2 and 4 mo after CI (b, d, and g; $n = 3$, $P < 0.0001$). In d, the low magnification EM insert shows that in mutant SNs, virtually all axons are engaged by SCs (arrowheads) but only very few went on to myelinate (arrow). (e) Tamoxifen (TAM) treatment does not affect myelination. (f) Noninjured mutant nerves collected 6 mo after tamoxifen induction show no structural abnormalities, implying that ILK is not necessary for the maintenance of the myelin membrane. (h) There was no difference in the axonal number in mutant crushed nerves when compared with control crushed nerves. (D) Oct6 immunohistochemistry on 2-mo post-CI cryosections. Oct6 is virtually absent in control nerves, whereas levels are still high in mutant nerves. Error bars indicate ± SEM. ***, $P < 0.001$. Bars: (C) 10 µm; (D) 50 µm.

the expression levels of PINCH1 and in AKT/PKB phosphorylation (Ser-473; Fig. 7 B). The loss of ILK did not affect the maintenance of the myelin membrane in noninjured nerves from tamoxifen-induced mutant mice (Fig. 7 C, f) nor did injection of tamoxifen impact on the myelination status of control nerves (Fig. 7 C, e). Distally from the crush site in injured nerves (Fig. 7 C, a–d), remyelination of mutant nerves was profoundly impaired (Fig. 7 C, b and d) compared with controls. Although these nerves contained sufficient numbers of SCs to engage virtually all axons (Fig. 7 C, d), a large proportion of SC–axon units were devoid of myelin sheaths (Fig. 7 C, g). Despite the deficits in remyelination, the number of axons per area in mutant nerves 4 mo after CI was not significantly different from that in control nerves (Fig. 7 C, h). Corroborating the morphological data, Oct6 immunoreactivity was markedly increased in mutant nerves at 2 mo after CI (Fig. 7 D).

These data suggest that ILK plays a direct role in SC remyelination but is not required for myelin maintenance. In the absence of ILK, remyelination of mutant crushed nerves was profoundly impaired. It is likely that this impairment is the result of a reduction in the levels of activity of signaling molecules, including AKT/PKB.

Discussion

We demonstrate that ILK plays an essential role in the regulation of radial sorting of axon bundles and in the remyelination of axons. During radial sorting of axon bundles, ILK negatively regulates Rho/ROCK signaling to control SC process extension. After SN CI, ILK facilitates axon remyelination presumably through the regulation of downstream signaling molecules such as AKT/PKB (Fig. 8).

ILK regulates radial sorting

Radial sorting is a key event in the development of the PNS. ECM–integrin interactions are important regulators of this process, and SC-specific ablation of laminins (Feltri and Wrabetz, 2005) or β1-integrin (Feltri et al., 2002) leads to defects in radial sorting. β1-integrin activates the small GTPase Rac1 to regulate radial sorting (Benninger et al., 2007; Nodari et al., 2007),

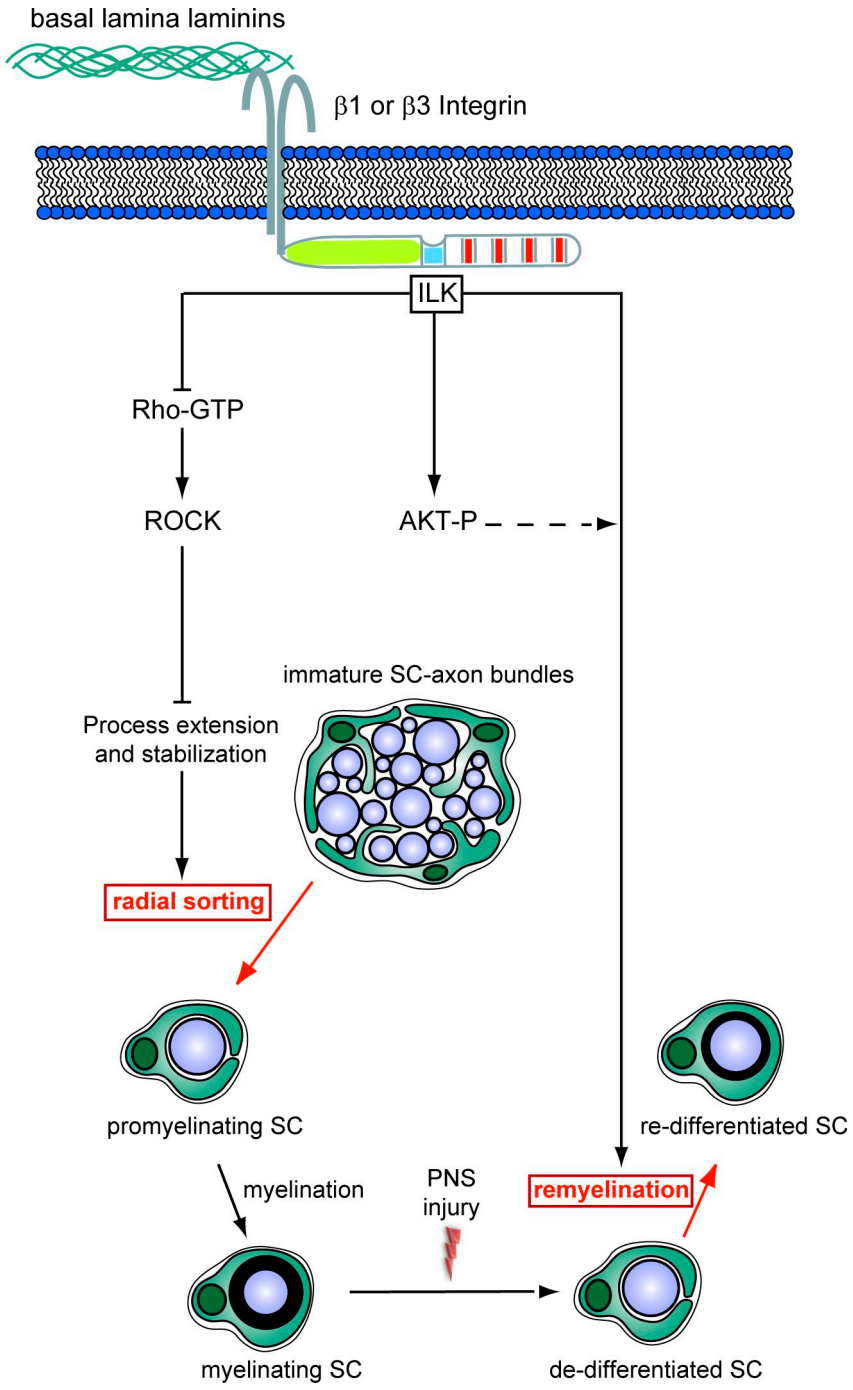

Figure 8. **Proposed mechanism for the regulation of SC development by ILK.** ILK plays distinct fundamental roles in the regulation of SC maturation. Early in development, ILK negatively regulates Rho/ROCK activity to trigger radial sorting. The phosphorylation of AKT on Ser-473 occurs in an ILK-dependent manner. On an adult animal after a nerve CI, ILK is also required for the transition from a promyelinating to a myelinating SC during remyelination. AKT activity is likely to also play an important role in this final differentiation step.

but the signaling pathways controlling this process remain largely unknown. We demonstrate that SC-specific ablation of *ILK*, an important regulator of integrin and growth factor–mediated signaling (Legate et al., 2006), profoundly impairs radial sorting in SNs. Dorsal and ventral nerve roots were also affected and contained several nonsorted axon bundles as well as 1:1 nonmyelinated profiles exhibiting empty loops of redundant BL (Fig. S1). Such BL protrusions are similar to those found in the SNs of β1-integrin and Rac1 SC-specific mutants (Feltri et al., 2002; Benninger et al., 2007; Nodari et al., 2007). SC proliferation is associated with radial sorting (Webster, 1971; Martin and Webster, 1973), and it is thought that a minimum threshold number of SCs is required to initiate this process. Ablation of genes involved in SC proliferation such as *Cdc42* (Benninger et al., 2007) or *FAK* (Grove et al., 2007) resulted in radial sorting impairment. In *ILK* mutant nerves, the numbers of SCs were normal and neither proliferation nor survival was affected. (Fig. S3, C–E). Therefore, and similarly to what has been postulated for *β1-integrin* (Feltri et al., 2002) and *Rac1* (Benninger et al., 2007; Nodari et al., 2007) mutant nerves, we consider it likely that the radial sorting impairment in ILK mutant nerves is a direct consequence of deficits in SC process extension. Our data supporting this view include (a) the inability of immature ILK-deficient SCs to completely envelop axon

bundles, (b) the formation of abnormal cytoplasmic protrusions projecting from the surface of ILK mutant SC–axon units, (c) the presence of layers of empty BL surrounding axon bundles and SC–axon units in *ILK* mutant nerves, suggesting failed attempts of mutant SCs to engage axon bundles and individual axons, (d) the finding that ILK mutant SCs plated on laminin-2, a component of SC BL, produced shorter processes compared with controls, and (e) the observation that the dynamics of process extension and retraction in mutant SCs was vastly increased as compared with controls.

The stability of the individual members of the IPP complex is dependent on the formation of the complex (Legate et al., 2006). In SCs, the loss of ILK resulted in reduced expression of other individual members of the IPP complex. Furthermore, the IPP complex can regulate the activity of Rho GTPases (Legate et al., 2006). We show that in ILK mutant nerves, the activities of Rac1, Cdc42, and Rho were increased compared with controls. Given that Rac1 activity is regulated by β1-integrin (Benninger et al., 2007; Nodari et al., 2007), the increase of activity of Rac1 in the absence of ILK was somewhat surprising. However, in addition to β1-integrin, ILK also binds directly to β3-integrin and indirectly to other receptors (Legate et al., 2006). This might explain why ILK regulation of Rac1 in particular, and Rho GTPases in general, does not mirror that of β1-integrin. In the PNS, the expression of RhoA, and of the two isoforms ROCK1 and ROCK2, is developmentally regulated, peaking at the onset of myelination and dropping afterward (Melendez-Vasquez et al., 2004). Other Rho proteins, i.e., RhoB and C, are also expressed in SCs (Terashima et al., 2001; Melendez-Vasquez et al., 2004), but their pattern of expression and specific functions are not known. Inhibition of ROCK by either Y27632 or fasudil restored process extension to mutant SCs in culture, suggesting that in SCs, ILK controls process extension mainly through regulation of Rho/ROCK activity.

ILK is known to negatively regulate Rho/ROCK activity by different mechanisms, including integrin-dependent FAK activation (Tahiliani et al., 1997; Wennerberg et al., 2000; Parsons, 2003) and paxillin phosphorylation (Chen et al., 2005). Negative regulation of Rho/ROCK activation by FAK might be dependent on FAK/Src phosphorylation of p190Rho–GTPase-activating protein (Schober et al., 2007) to promote Rho inactivation. In this study, we show that in ILK mutant nerve lysates, the activation of FAK, measured by a phospho-specific antibody recognizing the FAK autophosphorylation residue tyrosine 397, was significantly reduced as compared with controls. However, FAK appears to not regulate SC process extension, and SC-specific ablation of FAK mainly affects SC proliferation (Grove et al., 2007). Paxillin phosphorylation was also reduced in ILK mutant nerves. Paxillin is thought to participate in SC cytoskeletal reorganization (Chen et al., 2000), but its direct role in SC process extension has not been investigated. We also show in this study that RhoE expression is dramatically reduced in *ILK* mutant SCs. RhoE belongs to the Rnd subfamily of the Rho GTPases and, like the other subfamily members, binds but does not hydrolyze GTP (Riento et al., 2005). Therefore, it is not regulated by the classical GTP/GDP conformational switch of small Rho GTPases. RhoE exists in a GTP-bound state and antagonizes Rho/ROCK signaling (Riento et al., 2005) by binding and preventing ROCK I from interacting with its downstream targets (Riento et al., 2003). Our data, and the observation that short hairpin RNA–mediated knockdown of RhoE dramatically reduces process extension in primary rat SCs (our unpublished results), suggest that ILK regulation of RhoE is important in controlling SC process extension.

Finally, fasudil injections in mutant mice were sufficient to stimulate and reestablish radial sorting in mutant nerves. Together with our in vitro results, this supports the conclusion that inhibition of Rho/ROCK activity is essential to promote SC process extension and to initiate radial sorting. Other pathways than those regulated by ILK might also contribute to the negative regulation of Rho/ROCK signaling. Supporting this hypothesis is the observation that the mean length of SC processes in control cultures treated with Y27632 or fasudil was increased in relation to nontreated controls, indicating that the ILK-mediated inhibition of Rho/ROCK signaling was not complete.

ILK regulates remyelination

Stimulation of radial sorting by ROCK inhibition in ILK mutant nerves did not result in an increase in the number of myelinated fibers. This suggests that ILK function might be required for myelination of axons and that the signaling mechanisms for radial sorting and myelination of axons are likely to be different. This hypothesis is further supported by experiments using myelinating dorsal root ganglia (DRG) explant cultures derived from E13.5 mutant and control mice. In contrast to control DRG explant cultures, ILK mutant cultures largely failed to myelinate even after 10 d of continuous treatment with fasudil or Y27632 (Fig. S5).

The radial sorting phenotype of the *ILK* mutant prevented us from directly investigating the role of ILK in axonal myelination. Therefore, to address the role of ILK in myelin sheath formation independently of radial sorting, we used an inducible gene ablation system (Leone et al., 2003) followed by nerve crush. We demonstrate that after SN CI in adult mice, ILK-deficient SCs established 1:1 relations with axons, but a large proportion of axon–SC units failed to form myelin sheaths even 4 mo after CI. These findings indicate that at least during remyelination, ILK is required for the production of myelin sheaths.

ILK regulates AKT/PKB activation during PNS development

Phosphorylation of AKT/PKB can be regulated by the amount of neuregulin-1 type III present on the axon surface (Hu et al., 2006; Nave and Salzer, 2006) and is thought to be critical for SC myelination (Campana et al., 1999; Maurel and Salzer, 2000; Ogata et al., 2004; Nave and Salzer, 2006). Loss of ILK reduced the levels of AKT/PKB phosphorylation on Ser-473 but not on Thr-308 during PNS development. In fact, the levels of AKT/PKB phosphorylation on Thr-308 in mutant nerve lysates were even increased compared with controls. It is possible that increased phosphorylation on Thr-308 partially compensates for reduced AKT/PKB phosphorylation on Ser-473. However, if this is true, such compensation is likely to be ILK independent. In cancer cells, ILK specifically regulates the phosphorylation of Ser-473 but not of Thr-308 (McDonald et al., 2008), raising

the interesting possibility that Ser-473 phosphorylation may regulate different downstream targets than phosphorylation on Thr-308 under certain conditions. After CI, the levels of AKT/PKB phosphorylation on Ser-473 in tamoxifen-induced mutant nerve lysates were also reduced compared with controls. These results are consistent with the idea that ILK directly or indirectly regulates the phosphorylation of AKT/PKB on Ser-473. Based on this view, ILK can either function as a direct AKT/PKB Ser-473 kinase or be involved in the cellular regulation of putative AKT/PKB Ser-473 kinases (Hill et al., 2002). Although in macrophages (Troussard et al., 2003), oligodendrocytes (Chun et al., 2003), and primary skeletal muscle (Wang et al., 2008) the phosphorylation of AKT/PKB is dependent on ILK function, this requirement appears to be cell type specific. Loss of ILK did not change AKT/PKB phosphorylation in chondrocytes (Grashoff et al., 2003), keratinocytes (Lorenz et al., 2007), or nestin-positive neural progenitors (Mills et al., 2006). In addition to differentiation, the phosphorylation of AKT/PKB has been implicated in the control of SC proliferation and survival (Campana et al., 1999; Monje et al., 2006). However, in ILK mutant nerves, proliferation and survival was normal, indicating that the reduced levels of AKT/PKB phosphorylation were sufficient to promote SC proliferation and survival but not to support SC myelination.

In summary, we show that ILK and associated molecules of the IPP complex, functioning at the critical convergence of adhesion and growth factor signaling pathways, regulate radial sorting and remyelination of axons in the PNS. The multidimensional nature of this regulation is likely to rely on the activation of a multitude of different downstream pathways besides those controlling Rho/ROCK and AKT/PKB activation. To unveil these pathways in detail and to study their impact on PNS myelination and remyelination remains an important task for the future. This knowledge will be essential for our basic understanding of nerve biology in health and disease.

Materials and methods

Generation of conditional knockout mice

The generation of conditional *ILK* mutant has been described previously (Grashoff et al., 2003). Mice homozygous for the *ILK* floxed allele ($ILK^{lox/lox}$) were crossed with mice heterozygous for the floxed allele and additionally expressing the Cre recombinase under the control of the *Dhh* promoter ($Dhh\text{-}cre^{+}$ $ILK^{lox/w}$; Lindeboom et al., 2003) to obtain $Dhh\text{-}cre^{+}$ $ILK^{lox/lox}$ mice (hereafter called *ILK* mutant mice) and $Dhh\text{-}cre^{+}$ $ILK^{lox/wt}$ (hereafter called *ILK* control mice). Genotypes were determined by PCR on genomic DNA derived from tail biopsies. For remyelination experiments, the tamoxifen-inducible *PLP-CreERT2* line was used (Leone et al., 2003). The breeding strategy to produce inducible *ILK* mutant and control mice was the same as for *Dhh-cre ILK* mice.

EM

Mice were deeply anesthetized with 150 mg/kg pentobarbital i.p. (Nembutal; Abbott laboratories) and perfused with 0.1 M phosphate buffer, pH 7.4, followed by buffer containing 3% glutaraldehyde and 4% PFA. Fixed tissues were postfixed in 2% osmium tetroxide, dehydrated through a graded acetone series as described previously (Benninger et al., 2006), and embedded in Spurr's resin (Electron Microscopy Sciences). Semithin sections were stained with 1% Toluidine blue for analysis at the light microscope, and ultrathin sections were contrasted with 3% uranyl acetate and 1% lead citrate before observation in a transmission electron microscope (Morgagni 268; FEI).

Immunofluorescence and TUNEL staining

For Ki67 staining, frozen sections were submitted to antigen retrieval for 15 min at 90°C and stained as described previously (Benninger et al., 2007). For TUNEL staining, sections were fixed in 4% PFA for 10 min and blocked for 1 h with 10% goat serum, 1% Triton X-100, and 0.1% BSA in PBS. TUNEL assays were performed using indirect immunofluorescence to visualize nicked DNA according to the manufacturer's instructions (Roche). For Oct6, ILK, MBP, and RhoE staining, frozen sections were fixed in 4% PFA for 5 min and submitted to antigen retrieval in 10 mM citrate buffer for 5 min at 98°C. Sections were blocked (1 mg/ml of BSA in PBS with 0.05% Triton X-100) for 1 h at RT and incubated with mouse antibodies against ILK (1:200; BD), RhoE (1:200; Abcam), rat against MBP (1:50; AbD Serotec), or rabbit antibody against Oct6 (1:200; Ghazvini et al., 2002) overnight at 4°C. After washing in PBS, sections were incubated for 1 h at RT with antibody against mouse or rabbit coupled to Cy3 (1:300; Jackson ImmunoResearch Laboratories) and rat coupled to Alexa Fluor 488 (1:300; Invitrogen). Sections were washed with PBS, incubated for 5 min with DAPI, and mounted in Immu-Mount (Thermo Fisher Scientific).

Immunocytochemistry of SCs

Cultures were fixed in 4% PFA in microtubule protection (MP) buffer (65 mM Pipes, 25 mM Hepes, 10 mM EGTA, and 3 mM $MgCl_2$, pH 6.9) for 10 min at RT. The cells were permeabilized with 0.2% Triton X-100 in MP buffer for 5 min at RT and incubated with antibodies against ILK (1:200; BD), α-tubulin (1:100; Sigma-Aldrich), RhoE (1:200; Abcam), or S100 (1:200; Dako) overnight at 4°C. Cells were incubated with Cy3-conjugated anti–mouse (1:200; Jackson ImmunoResearch Laboratories), Alexa Fluor 488–conjugated anti–rabbit (1:200; Jackson ImmunoResearch Laboratories), or Alexa Fluor 488–conjugated phalloidin (1:100; Invitrogen) for 1 h at RT. Cells were washed in PBS, incubated with DAPI, and mounted in Immu-Mount.

Immunohistochemistry of DRG explant cultures

Cultures were fixed with 4% MP-PFA, postfixed in cold methanol (−20°C), washed in PBS, and blocked for 1 h at RT in 5% BSA, 0.1% goat serum, and 0.2% Triton X-100 in PBS. DRG cultures were incubated in primary antibody against MBP (1:200) overnight at 4°C before being washed in PBS and incubated with a Cy3-conjugated antibody (1:300; SMI 94; Jackson ImmunoResearch Laboratories). After washing, the cultures were incubated with DAPI, washed again, and mounted. Chemicals were obtained from Sigma-Aldrich unless stated otherwise.

All images were acquired at RT using fluorescence microscopes with 20×/0.4, 40×/0.6, or 100×/1.3 objectives (Vert Observer D1; Carl Zeiss, Inc.) or 20×/0.5, 40×/0.75, and 100×/1.3 objectives (Axioplan 2; Carl Zeiss, Inc.) equipped with charge-coupled device cameras (AxioCam HR or AxioCam MRm; Carl Zeiss, Inc.). Acquisition software was used (AxioVision 4.6; Carl Zeiss, Inc.). Images were further processed (levels adjusted) using Photoshop software (CS2; Adobe).

Mouse SC cultures

Primary mouse SC cultures were established from P0–P2 SNs as described previously (Benninger et al., 2007).

Mouse DRG dissociated explants

DRGs were obtained from E13.5 control and mutant mouse embryos. In brief, DRGs were digested in enzymatic digestion solution (0.25% trypsin-EDTA; Invitrogen) and plated overnight on matrigel-coated coverslips (two DRGs per coverslip) in C medium (10% FCS and 50 ng/ml neural growth factor [PeproTech] in DME-Glutamax [Invitrogen]) supplemented with 1% penicillin/streptomycin (Invitrogen). Then, medium was changed to NB medium (2% B27 supplement [Invitrogen], 4 g/liter D-glucose [Sigma-Aldrich], 2 mM L-glutamine [Invitrogen], and 50 ng/ml neural growth factor in Neurobasal [Invitrogen]). Myelination was induced over 10 consecutive days with C medium supplemented with 50 mg/ml ascorbic acid (Sigma-Aldrich) in some experiments in the presence of PBS, 10 µM Y27632 (Sigma-Alrich), or 40 µM fasudil (EMD).

Teased fibers preparation

Nerves of P24 control and mutant mice were extracted from the animals and fixed with 4% PFA in PBS for 2 h at 4°C. Meanwhile, glass slides (Erie Scientific) were coated with TESPA ((3-aminopropyl) triethoxysilane; Sigma-Aldrich) in the following procedure: 1 min in acetone and 1 min in 2% TESPA in acetone followed by two acetone washes of 30 s each. After 2 h fixation, the nerves were washed with PBS, stripped of perineurium and epineurium, and cut into small pieces. Individual fibers were sorted in PBS using two acupuncture needles (B-type; Seirin) on top of TESPA-coated glass slides. After teasing, the fibers were air dried and either stained immediately or stored at −20°C.

Immunostaining of teased fibers

Teased fibers were treated with prechilled acetone for 10 min, washed with PBS, and blocked in a buffer containing 5% fish gelatin (Sigma-Aldrich)

and 0.1% Triton X-100 in PBS for 1 h at room RT. Primary antibodies against ILK (1:200; BD), neurofilament M (1:200; Sigma-Aldrich), and E-cadherin (1:200; Enzo Biochem, Inc.) were incubated overnight on blocking buffer inside a wet chamber. The following morning, the fibers were washed and incubated with Cy3-conjugated anti–mouse (1:200; Jackson ImmunoResearch Laboratories), Cy2-conjugated anti–rat (1:200; Jackson ImmunoResearch Laboratories), and Cy5-conjugated anti–rabbit (1:50; Jackson ImmunoResearch Laboratories) at RT in blocking buffer. Fibers were washed in PBS, incubated with DAPI for 5 min, and after subsequent washing, mounted with Immu-Mount. Images were acquired at RT using a confocal microscope (SP1; Leica) using a 63×/0.6-1.32 objective and confocal software (LCS; Leica) in a sequential acquisition mode. Images were further processed (levels adjusted) using Photoshop software (CS2).

Quantitative real-time PCR

SNs were taken from P2 control and mutant mice, and total RNA was extracted using the RNeasy Mini kit (QIAGEN) according to their recommendations. cDNA was produced using SuperScript III Reverse Transcriptase (Invitrogen). Quantitative real-time PCR analyses were performed on a Sequence Detection System (ABI 7000; Applied Biosystems) using the 2× SYBR Green PCR Master Mix (Applied Biosystems) according to the manufacturer's recommendations. The amplification program was used for 5 min at 96°C, 40 steps of 30 s at 96°C, 30 s at 57°C, 30 s at 72°C, and 5 min at 72°C. The sequence of the primers used were as follows: glyceraldehyde 3-phosphate dehydrogenase (forward, 5′-CGTCCCGTAGACAAAATGGT-3′; reverse, 5′-TTGATGGCAACAATCTCCAC-3′), ILK (forward, 5′-TGGCTGGACAACACAGAAAA-3′; reverse, 5′-TGATCAGCATTTCAACCACC-3′), periaxin (forward, 5′-AGGAATCTTTGTCCGTGAGC-3′; reverse, 5′-AGAACACACGGGCACTCAG-3′), PMP22 (forward, 5′-GGGATCCTGTTCCTGCACAT-3′; reverse, 5′-TGCCAGAGATCAGTCGTGTGT-3′), P0/MPZ (forward, 5′-CCCTGGCCATTGTGGTTTAC-3′; reverse, 5′-CCATTCACTGGACCAGAAGGAG-3′), and myelin-associated glycoprotein (forward, 5′-CTGCCTTCAACCTGTCTGTG-3′; reverse, 5′-CGGGTTGGATTTTACCACAC-3′).

Western blot

Mice at different developmental stages were sacrificed, and SNs were dissected and separated from the epineurium and perineurium. They were homogenized with a chilled mortar and pestle in lysis buffer (0.1% SDS, 10 mM Tris-HCl, 150 mM NaCl, 50 mM NaF, 1 mM $NaVO_4$, 1 mM EDTA, 0.5% sodium-deoxycholate, and protease inhibitor cocktail [Sigma-Aldrich]). Extracts were processed using standard SDS-PAGE and Western blotting procedures. The following antibodies were used: ILK (1:1,000; BD), phosphorylated AKT Ser-473 (Cell Signaling Technology), phosphorylated AKT Thr-308 (1:1000; Cell Signaling Technology), AKT (1:1,000; Cell Signaling Technology), phosphorylated FAK tyrosine 397 (1:1,000; Millipore), FAK (1:1,000; Millipore), phosphorylated paxillin tyrosine 118 (1:1,000; BD), paxillin (1:1,000; Cell Signaling Technology), phosphorylated GSK3β Ser-9 (1:1,000; Cell Signaling Technology), GSK3 (1:1,000; Millipore), PINCH1 (1:10,000), PINCH2 (1:10,000), α-parvin (1:10,000), β-parvin (1:10,000), glyceraldehyde 3-phosphate dehydrogenase (1:20,000; HyTest), Rac1 (1:1,000; Millipore), Cdc42 (1:1,000; Abcam), RhoA/B/C (1:2,000; Millipore), and RhoE (1:1,000; Abcam). Secondary antibodies were obtained from Promega and SouthernBiotech. Bands were quantified using Quantity One software (Bio-Rad Laboratories).

Rho GTPase activity assay

GST–p21-activated kinase–crib domain construct was provided by J. Collard (The Netherlands Cancer Insitute, Amsterdam, Holland). GST-tagged rhotekin Rho-binding domain protein was purchased from Millipore. Cdc42, Rac1, and Rho activity were measured as described previously (Sander et al., 1998). In brief, SNs from at least three P5 mutant or control mice were pooled, homogenized in FISH buffer (10% glycerol, 50 mM Tris-HCl, pH 7.4, 100 mM NaCl, 1% NP-40, 2 mM $MgCl_2$, and protease inhibitor cocktail [Sigma-Aldrich]), and centrifuged for 5 min at 21,000 *g* at 4°C. Aliquots of exactly 10% of the volume were taken from the supernatant to determine the total protein amounts. The remaining supernatant was incubated with the bait proteins bound to glutathione-coupled Sepharose beads (GE Healthcare) at 4°C for 30 min. The beads and proteins bound to the fusion protein were washed three times in an excess of FISH buffer, eluted in Laemmli sample buffer, and analyzed for bound Cdc42, Rac1, or Rho molecules by Western blotting.

Nerve crush/remyelination assay

Using the inducible *PLP-CreERT2* transgene, SC-specific recombination of *ILK* was induced in 2-mo-old mutant and littermate control mice by a daily i.p. injection of 2 mg tamoxifen (Sigma-Aldrich) over five consecutive days. 8 wk after the last tamoxifen injection, we performed SN CIs to induce remyelination. Mice were anesthetized by a single i.p. injection of 65 mg/kg/bodyweight Ketamine (Ketaminol; Vetenaria) and 13 mg/kg/bodyweight Xylazine (Narcoxyl; Vetenaria). To prevent dehydration, a single i.p. injection of 1 ml Ringer's lactate solution (B. Braun Medical) was administered preoperatively. For analgesia, 0.1 mg/kg/bodyweight buprenorphinum (Temgesic; Essex Chemie) was injected just before the nerve crush and thereafter every 12 h for 2 d. SNs were analyzed distally from the crush site.

Morphometric analysis

The morphometric measurements in the fasudil experiment and the remyelination assays were performed in Toluidine blue–stained semithin sections (0.5 µm). For this purpose, a cross section per animal of the entire SN area was reconstructed by merging several high magnification photographs. The quantification of the 1:1 promyelinating cells, myelinated fibers, and axonal bundles was performed by counting all of the figures present in the entire SN cross section. The bundle area was quantified in pixels using Photoshop software (CS2) and converted to microns squared. The number of 1:1 and myelinated fibers was performed manually using the cell counter plugin from ImageJ software (click and count; National Institutes of Health). The quantification of SC process length in primary cultures was performed using ImageJ software in pixels and converted to microns.

Time-lapse microscopy

SCs were obtained from control and mutant SNs (Benninger et al., 2007) and plated on laminin substrates in media with or without ROCK inhibitors. SC cultures were imaged every 5 min over a period of 12 h in a live cell imaging station (37°C in 5% CO_2; CellR; Olympus) using the CellR acquisition software (Olympus) and a 20×/0.45 air objective (Olympus). The resulting photographic sequence was converted into a film (7 frames/s) using ImageJ (1.41). Quantification of process collapse events (process disappearing into the soma) was performed in films of three independent control and mutant cultures by tracking at least 10 cells per film.

Statistical analysis

The data show the mean ± SEM. Statistical significance was determined using a two-tailed Student's *t* test. Significance was set at $P < 0.05$, $P < 0.01$, or $P < 0.001$. *n* represents the number of independent experiments.

Online supplemental material

Fig. S1 shows radial sorting defects present in dorsal and ventral roots. Fig. S2 demonstrates that the myelinating SCs in mutant nerves are not recombined. Fig. S3 compares the differentiation, total cell number, proliferation, and apoptosis between control and *ILK* mutant SNs. Fig. S4 shows that FAK and paxillin activation and RhoE expression are reduced in mutant nerves as compared with controls. Fig. S5 shows that the continuous pharmacological inhibition of ROCK does not rescue myelination deficits in dissociated mutant DRG explant cultures. Videos 1–4 show that in *ILK* mutant SCs, the frequency of process extension and retraction is increased in relation to controls. Fasudil treatment abolishes those differences. Online supplemental material is available at http://www.jcb.org/cgi/content/full/jcb.200809008/DC1.

We thank members of the laboratories involved for many discussions, Hartmut Pohl for his help with EM, Harald Rauter for his assistance in live imaging, and Ned Mantei for critically reading the manuscript.

This study was supported by Technische Hochschule grants from the Eidgenössische Technische Hochschule Zurich (to Y. Benninger, T. Thurnherr, U. Suter, and J.B. Relvas) and by the Fundação para a Ciência e Tecnologia of Portugal (grants SFRH/BD/16677/2004 to J. Pereira and SFRH/BD/28640/2006 to A.F. Gonçalves), the Max Planck Society (grant to R. Fässler), the Swiss National Science Foundation, and the National Centre for Competence in Research in Neural Plasticity and Repair (grant to U. Suter).

Submitted: 1 September 2008
Accepted: 12 March 2009

References

Atanasoski, S., S.S. Scherer, E. Sirkowski, D. Leone, A.N. Garratt, C. Birchmeier, and U. Suter. 2006. ErbB2 signaling in Schwann cells is mostly dispensable for maintenance of myelinated peripheral nerves and proliferation of adult Schwann cells after injury. *J. Neurosci.* 26:2124–2131.

Benninger, Y., H. Colognato, T. Thurnherr, R.J. Franklin, D.P. Leone, S. Atanasoski, K.A. Nave, C. Ffrench-Constant, U. Suter, and J.B. Relvas. 2006. Beta1-integrin signaling mediates premyelinating oligodendrocyte survival but is not required for CNS myelination and remyelination. *J. Neurosci.* 26:7665–7673.

Benninger, Y., T. Thurnherr, J.A. Pereira, S. Krause, X. Wu, A. Chrostek-Grashoff, D. Herzog, K.A. Nave, R.J. Franklin, D. Meijer, et al. 2007. Essential and distinct roles for cdc42 and rac1 in the regulation of Schwann cell biology during peripheral nervous system development. *J. Cell Biol.* 177:1051–1061.

Campana, W.M., S.J. Darin, and J.S. O'Brien. 1999. Phosphatidylinositol 3-kinase and Akt protein kinase mediate IGF-I- and prosaptide-induced survival in Schwann cells. *J. Neurosci. Res.* 57:332–341.

Chen, G.C., B. Turano, P.J. Ruest, M. Hagel, J. Settleman, and S.M. Thomas. 2005. Regulation of Rho and Rac signaling to the actin cytoskeleton by paxillin during *Drosophila* development. *Mol. Cell. Biol.* 25:979–987.

Chen, L.M., D. Bailey, and C. Fernandez-Valle. 2000. Association of beta 1 integrin with focal adhesion kinase and paxillin in differentiating Schwann cells. *J. Neurosci.* 20:3776–3784.

Chen, Z.L., W.M. Yu, and S. Strickland. 2007. Peripheral regeneration. *Annu. Rev. Neurosci.* 30:209–233.

Chun, S.J., M.N. Rasband, R.L. Sidman, A.A. Habib, and T. Vartanian. 2003. Integrin-linked kinase is required for laminin-2–induced oligodendrocyte cell spreading and CNS myelination. *J. Cell Biol.* 163:397–408.

Colognato, H., C. ffrench-Constant, and M.L. Feltri. 2005. Human diseases reveal novel roles for neural laminins. *Trends Neurosci.* 28:480–486.

Feltri, M.L., and L. Wrabetz. 2005. Laminins and their receptors in Schwann cells and hereditary neuropathies. *J. Peripher. Nerv. Syst.* 10:128–143.

Feltri, M.L., D. Graus Porta, S.C. Previtali, A. Nodari, B. Migliavacca, A. Cassetti, A. Littlewood-Evans, L.F. Reichardt, A. Messing, A. Quattrini, et al. 2002. Conditional disruption of β1 integrin in Schwann cells impedes interactions with axons. *J. Cell Biol.* 156:199–209.

Ghazvini, M., W. Mandemakers, M. Jaegle, M. Piirsoo, S. Driegen, M. Koutsourakis, X. Smit, F. Grosveld, and D. Meijer. 2002. A cell type-specific allele of the POU gene Oct-6 reveals Schwann cell autonomous function in nerve development and regeneration. *EMBO J.* 21:4612–4620.

Grashoff, C., A. Aszodi, T. Sakai, E.B. Hunziker, and R. Fassler. 2003. Integrin-linked kinase regulates chondrocyte shape and proliferation. *EMBO Rep.* 4:432–438.

Grove, M., N.H. Komiyama, K.A. Nave, S.G. Grant, D.L. Sherman, and P.J. Brophy. 2007. FAK is required for axonal sorting by Schwann cells. *J. Cell Biol.* 176:277–282.

Hannigan, G.E., C. Leung-Hagesteijn, L. Fitz-Gibbon, M.G. Coppolino, G. Radeva, J. Filmus, J.C. Bell, and S. Dedhar. 1996. Regulation of cell adhesion and anchorage-dependent growth by a new beta 1-integrin-linked protein kinase. *Nature.* 379:91–96.

Hill, M.M., J. Feng, and B.A. Hemmings. 2002. Identification of a plasma membrane Raft-associated PKB Ser473 kinase activity that is distinct from ILK and PDK1. *Curr. Biol.* 12:1251–1255.

Hu, X., C.W. Hicks, W. He, P. Wong, W.B. Macklin, B.D. Trapp, and R. Yan. 2006. Bace1 modulates myelination in the central and peripheral nervous system. *Nat. Neurosci.* 9:1520–1525.

Hynes, R.O. 1992. Integrins: versatility, modulation, and signaling in cell adhesion. *Cell.* 69:11–25.

Indra, A.K., X. Warot, J. Brocard, J.M. Bornert, J.H. Xiao, P. Chambon, and D. Metzger. 1999. Temporally-controlled site-specific mutagenesis in the basal layer of the epidermis: comparison of the recombinase activity of the tamoxifen-inducible Cre-ER(T) and Cre-ER(T2) recombinases. *Nucleic Acids Res.* 27:4324–4327.

Joseph, N.M., Y.S. Mukouyama, J.T. Mosher, M. Jaegle, S.A. Crone, E.L. Dormand, K.F. Lee, D. Meijer, D.J. Anderson, and S.J. Morrison. 2004. Neural crest stem cells undergo multilineage differentiation in developing peripheral nerves to generate endoneurial fibroblasts in addition to Schwann cells. *Development.* 131:5599–5612.

Legate, K.R., E. Montanez, O. Kudlacek, and R. Fassler. 2006. ILK, PINCH and parvin: the tIPP of integrin signalling. *Nat. Rev. Mol. Cell Biol.* 7:20–31.

Leone, D.P., S. Genoud, S. Atanasoski, R. Grausenburger, P. Berger, D. Metzger, W.B. Macklin, P. Chambon, and U. Suter. 2003. Tamoxifen-inducible glia-specific Cre mice for somatic mutagenesis in oligodendrocytes and Schwann cells. *Mol. Cell. Neurosci.* 22:430–440.

Li, M., A.K. Indra, X. Warot, J. Brocard, N. Messaddeq, S. Kato, D. Metzger, and P. Chambon. 2000. Skin abnormalities generated by temporally controlled RXRalpha mutations in mouse epidermis. *Nature.* 407:633–636.

Lindeboom, F., N. Gillemans, A. Karis, M. Jaegle, D. Meijer, F. Grosveld, and S. Philipsen. 2003. A tissue-specific knockout reveals that Gata1 is not essential for Sertoli cell function in the mouse. *Nucleic Acids Res.* 31:5405–5412.

Lorenz, K., C. Grashoff, R. Torka, T. Sakai, L. Langbein, W. Bloch, M. Aumailley, and R. Fassler. 2007. Integrin-linked kinase is required for epidermal and hair follicle morphogenesis. *J. Cell Biol.* 177:501–513.

Luo, L. 2002. Actin cytoskeleton regulation in neuronal morphogenesis and structural plasticity. *Annu. Rev. Cell Dev. Biol.* 18:601–635.

Martin, J.R., and H.D. Webster. 1973. Mitotic Schwann cells in developing nerve: their changes in shape, fine structure, and axon relationships. *Dev. Biol.* 32:417–431.

Maurel, P., and J.L. Salzer. 2000. Axonal regulation of Schwann cell proliferation and survival and the initial events of myelination requires PI 3-kinase activity. *J. Neurosci.* 20:4635–4645.

McDonald, P.C., A. Oloumi, J. Mills, I. Dobreva, M. Maidan, V. Gray, E.D. Wederell, M.B. Bally, L.J. Foster, and S. Dedhar. 2008. Rictor and integrin-linked kinase interact and regulate Akt phosphorylation and cancer cell survival. *Cancer Res.* 68:1618–1624.

Melendez-Vasquez, C.V., S. Einheber, and J.L. Salzer. 2004. Rho kinase regulates schwann cell myelination and formation of associated axonal domains. *J. Neurosci.* 24:3953–3963.

Mills, J., A. Niewmierzycka, A. Oloumi, B. Rico, R. St-Arnaud, I.R. Mackenzie, N.M. Mawji, J. Wilson, L.F. Reichardt, and S. Dedhar. 2006. Critical role of integrin-linked kinase in granule cell precursor proliferation and cerebellar development. *J. Neurosci.* 26:830–840.

Monje, P.V., M. Bartlett Bunge, and P.M. Wood. 2006. Cyclic AMP synergistically enhances neuregulin-dependent ERK and Akt activation and cell cycle progression in Schwann cells. *Glia.* 53:649–659.

Mueller, B.K., H. Mack, and N. Teusch. 2005. Rho kinase, a promising drug target for neurological disorders. *Nat. Rev. Drug Discov.* 4:387–398.

Nave, K.A., and J.L. Salzer. 2006. Axonal regulation of myelination by neuregulin 1. *Curr. Opin. Neurobiol.* 16:492–500.

Nodari, A., D. Zambroni, A. Quattrini, F.A. Court, A. D'Urso, A. Recchia, V.L. Tybulewicz, L. Wrabetz, and M.L. Feltri. 2007. β1 integrin activates Rac1 in Schwann cells to generate radial lamellae during axonal sorting and myelination. *J. Cell Biol.* 177:1063–1075.

Ogata, T., S. Iijima, S. Hoshikawa, T. Miura, S. Yamamoto, H. Oda, K. Nakamura, and S. Tanaka. 2004. Opposing extracellular signal-regulated kinase and Akt pathways control Schwann cell myelination. *J. Neurosci.* 24:6724–6732.

Parsons, J.T. 2003. Focal adhesion kinase: the first ten years. *J. Cell Sci.* 116:1409–1416.

Persad, S., S. Attwell, V. Gray, N. Mawji, J.T. Deng, D. Leung, J. Yan, J. Sanghera, M.P. Walsh, and S. Dedhar. 2001. Regulation of protein kinase B/Akt-serine 473 phosphorylation by integrin-linked kinase: critical roles for kinase activity and amino acids arginine 211 and serine 343. *J. Biol. Chem.* 276:27462–27469.

Riento, K., and A.J. Ridley. 2003. Rocks: multifunctional kinases in cell behaviour. *Nat. Rev. Mol. Cell Biol.* 4:446–456.

Riento, K., R.M. Guasch, R. Garg, B. Jin, and A.J. Ridley. 2003. RhoE binds to ROCK I and inhibits downstream signaling. *Mol. Cell. Biol.* 23:4219–4229.

Riento, K., P. Villalonga, R. Garg, and A. Ridley. 2005. Function and regulation of RhoE. *Biochem. Soc. Trans.* 33:649–651.

Rosenberger, G., I. Jantke, A. Gal, and K. Kutsche. 2003. Interaction of alphaPIX (ARHGEF6) with beta-parvin (PARVB) suggests an involvement of alphaPIX in integrin-mediated signaling. *Hum. Mol. Genet.* 12:155–167.

Sander, E.E., S. van Delft, J.P. ten Klooster, T. Reid, R.A. van der Kammen, F. Michiels, and J.G. Collard. 1998. Matrix-dependent Tiam1/Rac signaling in epithelial cells promotes either cell-cell adhesion or cell migration and is regulated by phosphatidylinositol 3-kinase. *J. Cell Biol.* 143:1385–1398.

Schober, M., S. Raghavan, M. Nikolova, L. Polak, H.A. Pasolli, H.E. Beggs, L.F. Reichardt, and E. Fuchs. 2007. Focal adhesion kinase modulates tension signaling to control actin and focal adhesion dynamics. *J. Cell Biol.* 176:667–680.

Shimokawa, H., K. Hiramori, H. Iinuma, S. Hosoda, H. Kishida, H. Osada, T. Katagiri, K. Yamauchi, Y. Yui, T. Minamino, et al. 2002. Anti-anginal effect of fasudil, a Rho-kinase inhibitor, in patients with stable effort angina: a multicenter study. *J. Cardiovasc. Pharmacol.* 40:751–761.

Tahiliani, P.D., L. Singh, K.L. Auer, and S.E. LaFlamme. 1997. The role of conserved amino acid motifs within the integrin beta3 cytoplasmic domain in triggering focal adhesion kinase phosphorylation. *J. Biol. Chem.* 272:7892–7898.

Terashima, T., H. Yasuda, M. Terada, S. Kogawa, K. Maeda, M. Haneda, A. Kashiwagi, and R. Kikkawa. 2001. Expression of Rho-family GTPases (Rac, cdc42, RhoA) and their association with p-21 activated kinase in adult rat peripheral nerve. *J. Neurochem.* 77:986–993.

Troussard, A.A., N.M. Mawji, C. Ong, A. Mui, R. St -Arnaud, and S. Dedhar. 2003. Conditional knock-out of integrin-linked kinase demonstrates an essential role in protein kinase B/Akt activation. *J. Biol. Chem.* 278:22374–22378.

Tu, Y., F. Li, and C. Wu. 1998. Nck-2, a novel Src homology2/3-containing adaptor protein that interacts with the LIM-only protein PINCH and components of growth factor receptor kinase-signaling pathways. *Mol. Biol. Cell.* 9:3367–3382.

Wang, H.V., L.W. Chang, K. Brixius, S.A. Wickstrom, E. Montanez, I. Thievessen, M. Schwander, U. Muller, W. Bloch, U. Mayer, and R. Fassler. 2008. Integrin-linked kinase stabilizes myotendinous junctions and protects muscle from stress-induced damage. *J. Cell Biol.* 180:1037–1049.

Webster, H.D. 1971. The geometry of peripheral myelin sheaths during their formation and growth in rat sciatic nerves. *J. Cell Biol.* 48:348–367.

Wennerberg, K., A. Armulik, T. Sakai, M. Karlsson, R. Fassler, E.M. Schaefer, D.F. Mosher, and S. Johansson. 2000. The cytoplasmic tyrosines of integrin subunit beta1 are involved in focal adhesion kinase activation. *Mol. Cell. Biol.* 20:5758–5765.

Pereira et al., http://www.jcb.org/cgi/content/full/jcb.200809008/DC1

JCB

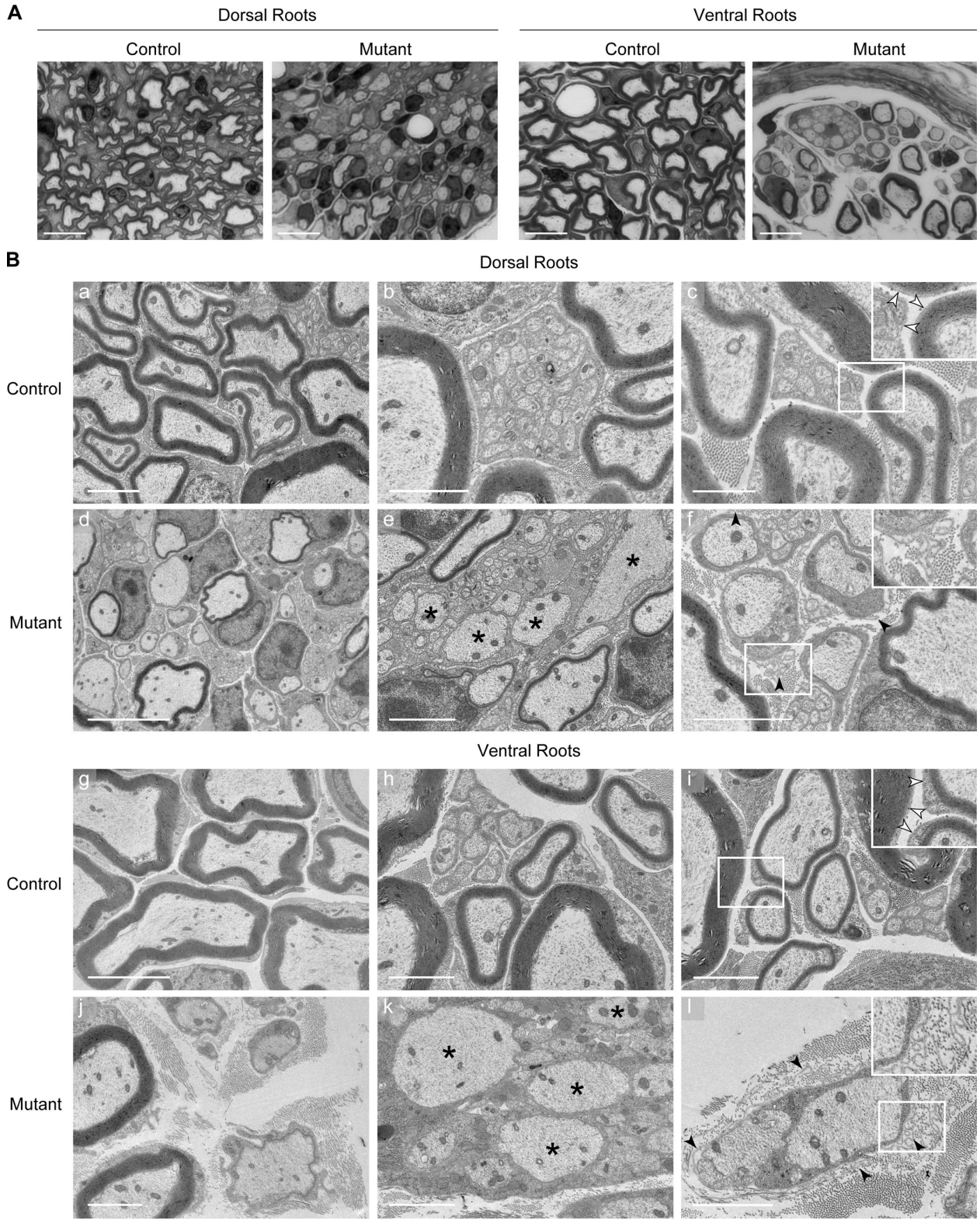

Figure S1. **Radial sorting defects present in dorsal and ventral roots.** (A) Toluidine blue–stained semithin sections of dorsal and ventral roots obtained from control and *ILK* mutant mice at P24. The overview shows that the roots of the mutant animals are hypomyelinated. Bars, 10 µm. (B) Electron micrographs of dorsal (a–f) and ventral (g–l) roots of P24 control and *ILK* mutant animals. In controls, both dorsal and ventral roots are myelinated (a and g), and the axons below the size threshold for sorting and myelination are engaged by nonmyelinating SCs (b and h). (d and j) In *ILK* mutants, there are multiple axons in a 1:1 relation with SCs that are not myelinated. (e and h) Additionally, in both dorsal and ventral roots there are bundles of axons not sorted by SCs (asterisks), some of which are above the size threshold for myelination. Finally, control SCs in dorsal and ventral roots display a BL tightly apposed to the plasma membrane (c and i, white arrowheads), whereas mutant cells present loops of detached BL and sometimes even multiple layers of BL (f and l, back arrowheads). Boxed regions indicate higher magnification areas, presented as insets. Bars: (a, c, e, f, and h–l) 2 µm; (b) 1 µm; (d and g) 5 µm.

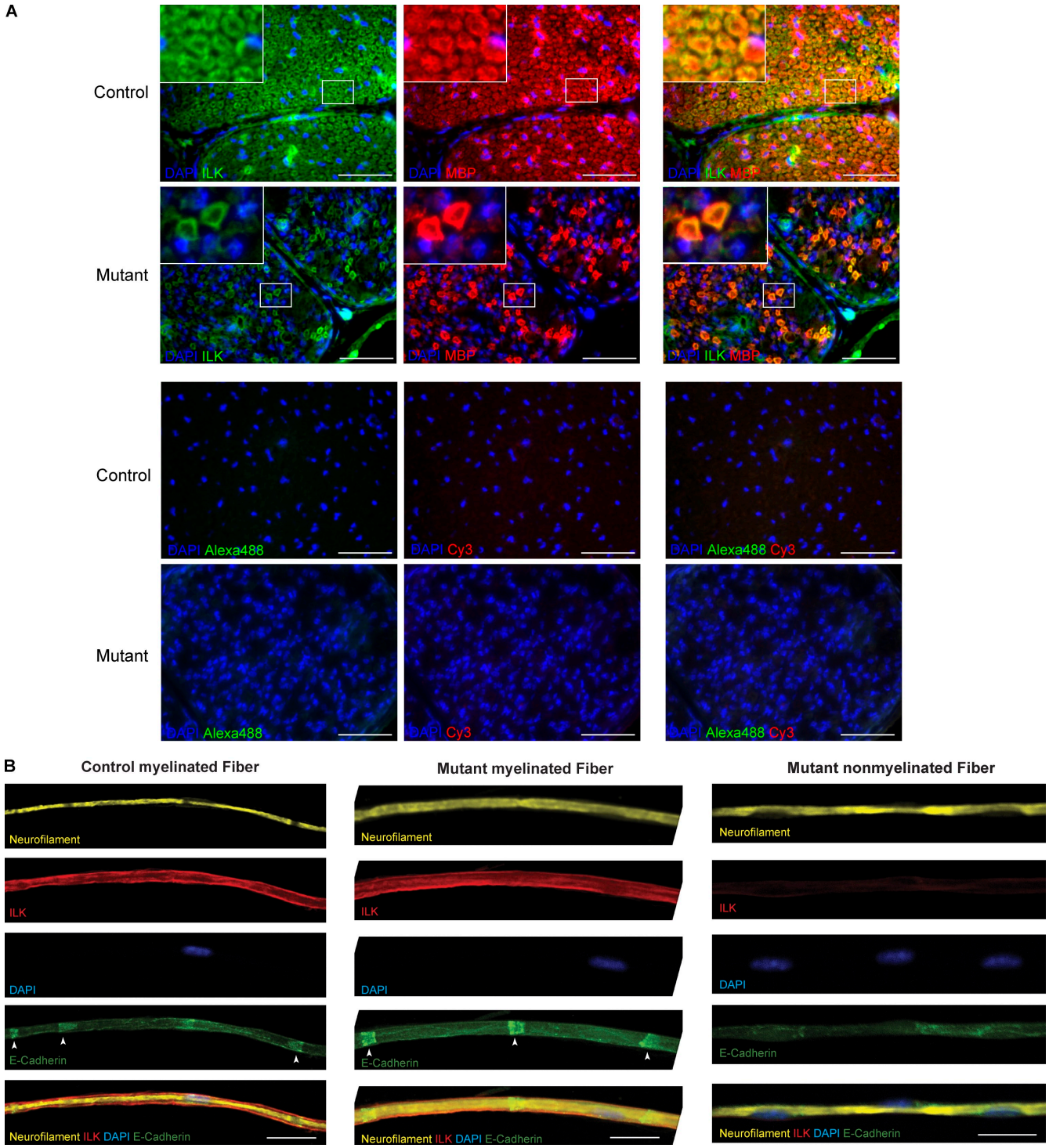

Figure S2. **Myelinating SCs in mutant nerves were not recombined.** (A) Immunohistochemistry on P24 mutant and control SN cryosections using antibodies against ILK and MBP. Only unrecombined ILK-positive cells are MBP positive in mutant nerves. Secondary antibody incubation does not reveal any specific signal. The apparent localization of ILK in the compact myelin is most likely to be caused by the antigen retrieval process necessary to obtain staining. Bars, 50 µm. (B) Teased fibers obtained from P24 control and mutant mice were stained with neurofilament, E-cadherin, ILK, and DAPI and photographed with a confocal microscope. In control and mutant myelinated fibers, E-cadherin is organized at the Schmidt-Lanterman incisures in a typical v-shape fashion (arrowheads). In the absence of myelin and of incisures, E-cadherin is disorganized. Myelinated fibers in control and mutant fibers are ILK positive, whereas nonmyelinated mutant fibers engaged by SCs are ILK negative. Boxed regions indicate higher magnification areas, presented as insets. Bars, 8 µm.

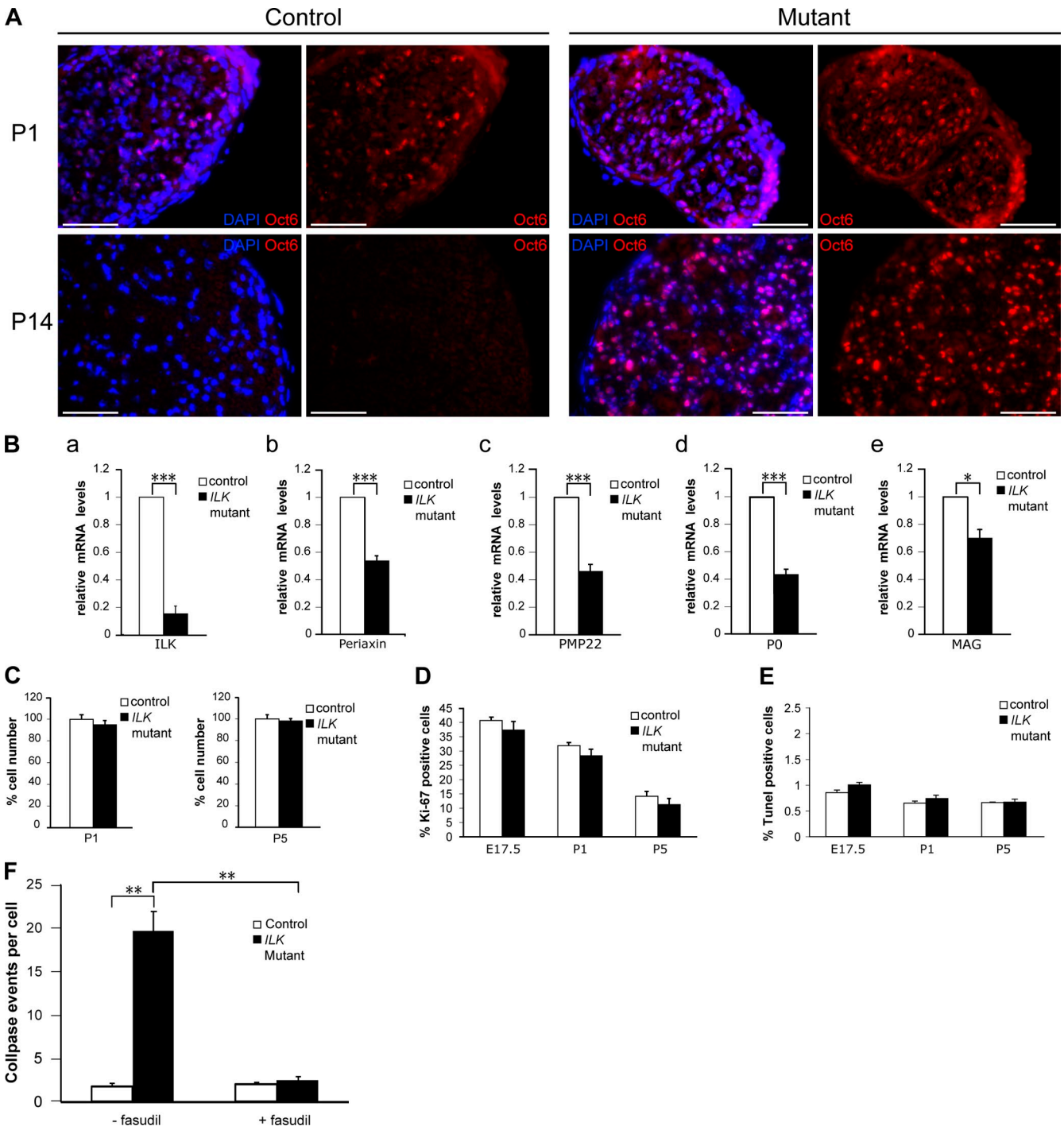

Figure S3. **Differentiation, total cell number, proliferation, and apoptosis in *ILK* mutant SNs.** Mutant SCs display increased process instability associated with ROCK signaling. (A) Oct6 immunohistochemistry on cross sections of frozen SNs obtained from P1 and P14 control and mutant mice. Oct6 expression peaks in promyelinating SCs and decreases at the onset of myelination. At P1, Oct6 is detected in both control and mutant nerves. At P14, the protein is no longer detected in control nerves, but it remains abundant in mutant nerves. (B) Real-time PCR performed on P2 SNs. (a) *ILK* mRNA is reduced in mutant nerves ($n = 4$, $P_{ILK} < 0.0001$). (b–e) The mRNA levels of *Periaxin* (b; $n = 3$, $P_{periaxin} = 0.00030$), *PMP22* (c; $n = 3$, $P_{PMP22} = 0.00043$), *P0* (d; $n = 3$, $P_{P0} = 0.00012$), and *MAG* (e; $n = 3$, $P_{MAG} = 0.010$) are significantly reduced in mutant nerves as compared with controls. (C) The percentage of cells present in the distal part of the SNs from control and mutant mice is not significantly different. (D) The percentage of Ki-67–positive cells is similar in control and mutant nerves, suggesting normal SC proliferation in the absence of ILK. (E) The percentage of TUNEL-positive apoptotic cells is not significantly altered in *ILK* mutant SN as compared with controls. (F) ILK control and mutant SCs were photographed every 5 min over a period of 12 h. Multiple SCs (10 per video, three independent videos per condition) were followed through every frame, and the complete retraction events (when the process disappears into the cell body) were quantified. The number of complete retraction events in mutant SC cultures was eightfold higher than in their control counterparts ($n = 3$, $P = 0.0012$). When treated with fasudil, mutant cultures display a significantly lower rate of retraction events compared with non-treated mutant cultures ($n = 3$, $P = 0.0014$). Error bars display ± SEM. *, $P < 0.05$; **, $P < 0.01$; ***, $P < 0.001$. Bars, 50 µm.

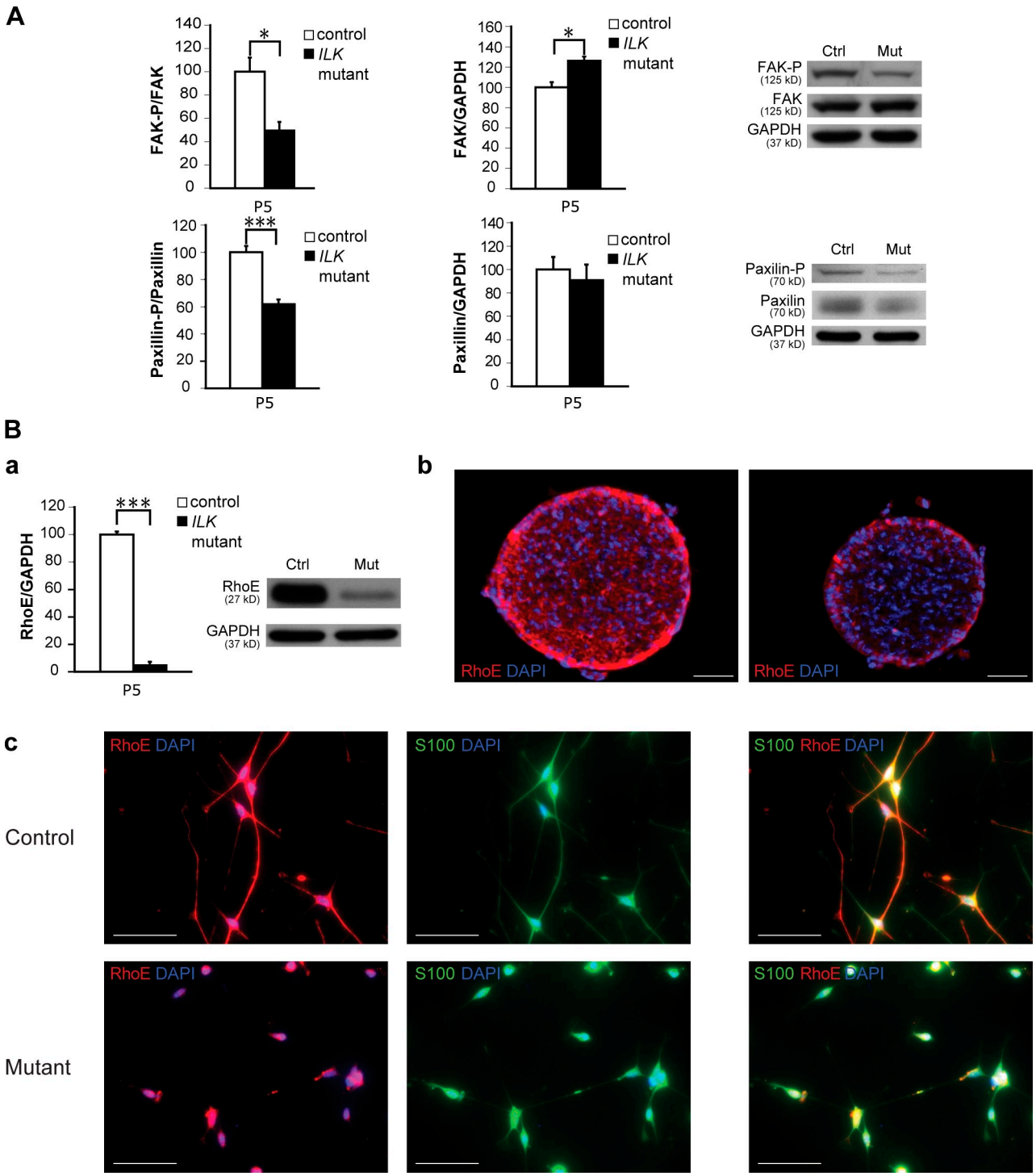

Figure S4. **Reduced FAK and paxillin activation and RhoE expression in the absence of ILK.** (A) Western blot analysis of SN lysates at P5. Levels of FAK ($n = 4$, $P = 0.012$) and paxillin ($n = 3$, $P = 0.0026$) phosphorylation are reduced. Total levels of FAK are slightly increased ($n = 4$, $P = 0.023$). FAK-P, phosphorylated FAK; paxillin-P, phosphorylated paxillin. Error bars display ± SEM. (B) Western blot analysis of protein lysates from control (ctrl) and mutant (mut) SNs at P5. (a) RhoE is dramatically reduced in mutant lysates as compared with controls ($n = 3$, $P < 0.0001$). (b) Immunohistochemistry on cross sections of control and *ILK* mutant SNs shows reduction of RhoE compared with controls. (c) RhoE immunoreactivity is also reduced in mutant SCs in culture compared with controls. Note that in control SCs, RhoE is present in the processes, whereas in mutant cells, RhoE is predominantly localized in the perinuclear region. Error bars display ± SEM. *, $P < 0.05$; ***, $P < 0.001$. Bars, 50 µm.

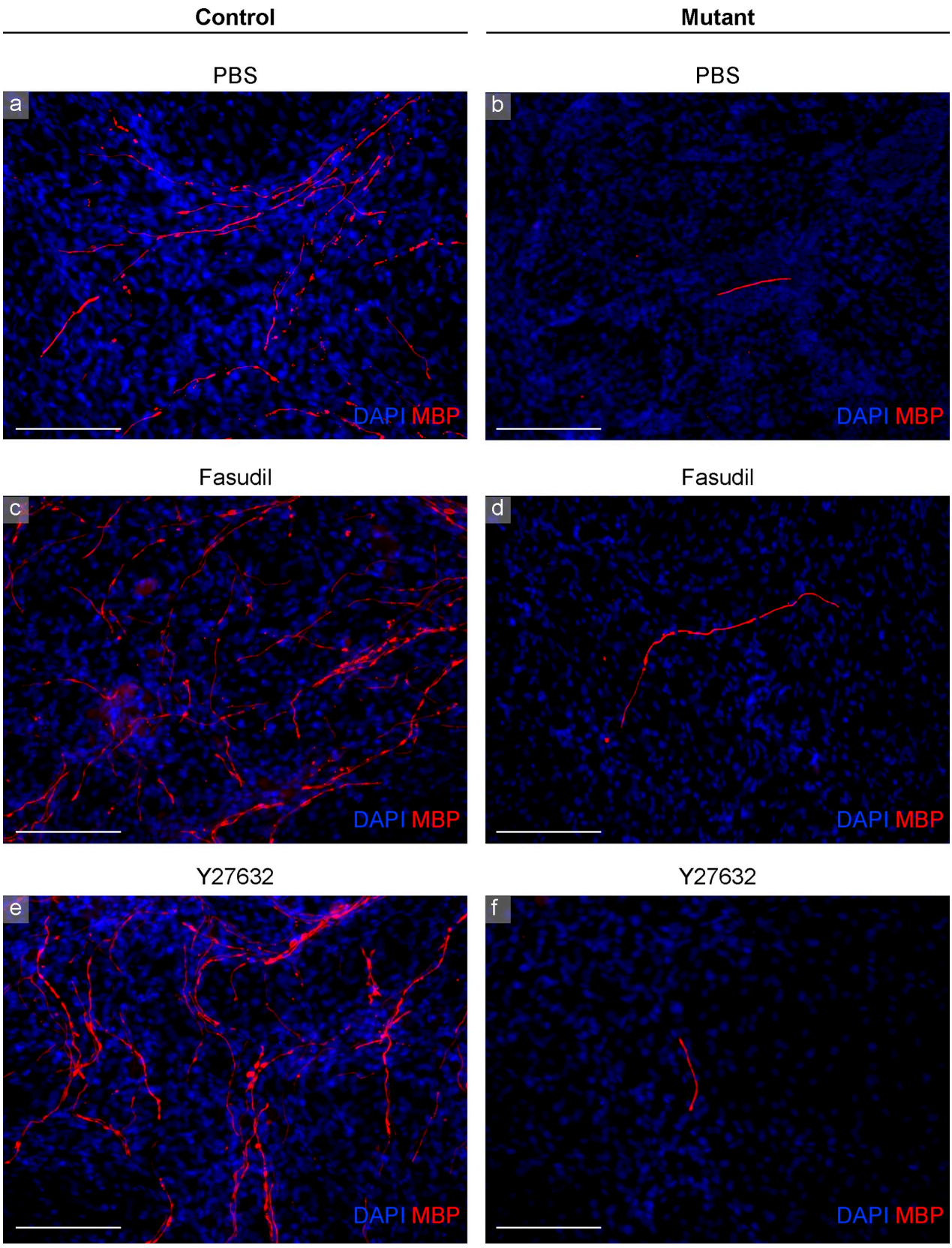

Figure S5. **Continuous pharmacological inhibition of ROCK does not rescue myelination deficits in dissociated *ILK* mutant DRG explants.** DRG from E13.5 control and mutant mice were dissociated and cultured for 17 d. After induction of myelination, the cultures were treated with fasudil, Y27632, or PBS for 10 consecutive days. (a and b) In vitro myelination of mutant cultures is severely impaired when compared with controls. (c–f) Although inhibition of ROCK signaling induces increased myelination in control cultures (c and e), as reported previously (Melendez-Vasquez, C.V., S. Einheber, and J.L. Salzer. 2004. *J. Neurosci.* 24:3953–3963), it fails to restore myelination to mutant cultures (d and f). Bars, 100 µm.